THE IDENTIFICATION OF INHOMOGENEITIES FOR TUMOR DOSE
CALCULATIONS DURING TREATMENT PLANNING

BY

Francis Joseph Bova

A DISSERTATION PRESENTED TO THE GRADUATE COUNCIL OF
THE UNIVERSITY OF FLORIDA
IN PARTIAL FULFILLMENT OF THE REQUIREMENTS FOR THE
DEGREE OF DOCTOR OF PHILOSOPHY

UNIVERSITY OF FLORIDA
1977

To my parents without whose support and many
sacrifices my education would not
have been possible.

ACKNOWLEDGEMENTS

I would like to express my sincere appreciation to my advisory committee for their help and guidance throughout this work. I would like to give special thanks to my committee chairman, Dr. Walter Hauderli, for his help and guidance with this project and to Dr. Rodney Million for his support, both financial and moral, and for providing an educational atmosphere without which this research would never have been possible. I would also like to thank Drs. Genevieve Roessler, Charles Roessler and Hugh Campbell for their guidance throughout my graduate career at the University of Florida.

I feel as though I can never adequately give thanks to Dr. Lawrence Fitzgerald who not only made himself available at all hours for advice and guidance over the last three years, and who has spent many laborious hours wading through the early drafts of this manuscript, but because of whom this research effort has been an enjoyable and personally rewarding educational experience. I sincerely feel that without his friendship and guidance, this work would never have been possible.

I would like to give special thanks to Barbara Smith whose support and companionship throughout the last two years of this work has so greatly influenced my life.

Sincere thanks go to Amy Tanner for her assistance in typing the final manuscript and my sincerest appreciation goes to Denise Keefer for her patience throughout the working drafts and the excellent job on the final manuscript.

TABLE OF CONTENTS

THE IDENTIFICATION OF INHOMOGENEITIES FOR TUMOR DOSE
CALCULATION DURING TREATMENT PLANNING

by

Francis Joseph Bova

December, 1977

Chairman: Walter Mauderli, D. Sc.
Co-Chairman: Lawrence T. Fitzgerald, Ph. D.
Major Department: Nuclear Engineering Sciences

The purpose of this work was to develop an apparatus which de-
lineated the linear attenuation coefficient and position of anatomical
inhomogeneities for routine clinical use in radiotherapy. A whole-
body cobalt-60 axial tomographic scanner has been designed and built
to fulfill this objective.

The criteria of overall low cost, simplicity of operation, and
the ability to interface easily with the department's existing system
has been used. The scanner has therefore been designed around a low
cost dedicated digital computer.

Cobalt-60 was chosen as the source of the scanning beam in an
effort to minimize the scaling of data to the regions of interaction
used in routine radiotherapy.

Because of the heavy, bulky shielding usually associated with
cobalt-60 sources, a special collimator shield was designed. It was
fabricated from depleted uranium. The design incorporates a fixed,
1.98 millimeter, straight-bore collimator with a source which is doubly
encapsulated onto a sliding tungsten rod. When the rod is pulled back
one centimeter from the resting position, the source aligns with the

collimator hole and is considered "on." The detector, mounted opposite the source, is a 4 inch long sodium iodide crystal, with interchange-able straight-bore collimators.

Both the collimator shield and detector are moved across the region of interest by stepping motors, gear reduction units, and precision ball screws. This arrangement is used to assure accurate transverse motion with a minimum of computer control. After a trans-verse scan has been completed, the apparatus is rotated on a large 54 inch diameter wheel. This rotation will again be controlled by stepping motors and gear reduction units. The width of the transverse scan is variable, as is the number of degrees per angular rotation. The transmission data are collected on a 3.3 millimeter grid, and the reconstruction is performed on a one-quarter inch grid. The grid size can readily be altered and is only dependent upon the number of trans-mission measurements taken. The data are recorded on a computer-compatible, write-only, tape recorder. Once the data are complete, the tape can be transferred to the departments time-sharing computer.

The raw data are then reconstructed by an algorithm using filtered back projections. A treatment planning algorithm will then utilize these data to correct internal dose distributions.

CHAPTER 1

INTRODUCTION

The path which radiation treatment planning has followed is not
unlike that of many other branches of science. The need to understand
a physical phenomenon prompted a scientific investigation with the
object of a delineation of parameters which affect its interaction. The
end goal of this investigation has been the formulation of these para-
meters into mathematical expressions with which the phenomenon can be
predicted.

The early days of treatment planning saw crude and inexact tech-
niques employed, such as calibrations of radiation fields by means of
erythemal levels. Today these calibrations are performed with sophis-
ticated equipment which allows higher degrees of precision and accuracy.
The state of the art for obtaining radiation dose distributions within
a patient involves several steps, the first of which is the measuring
of radiation field profiles. These profiles are commonly known as
isodose curves and are obtained with the use of tissue-equivalent
phantoms. These phantoms are usually rectangular Lucite tanks filled
with water. Since the skin surfaces of patients who must be irradi-
ated are normally not flat, a two-dimensional contour, of the surface
upon which the radiation field will be imposed, is taken. The original
beam profile is then adjusted so that it resembles the profile which
would have been measured if the phantom had the identical surface contour
as that of the patient.

Most planning procedures stop at this level of sophistication, although with use of only the aforementioned procedure, known inaccuracies exist in the dosimetric process. X and gamma rays used in radiation therapy are absorbed primarily through Compton's interaction, which is dependent upon electron density. With the exception of hydrogen, all elements have essentially the same number of electrons per mole or per gram/centimeter^2. If all anatomical structures had identical densities, the water tank phantom would be accurate; however, various structures within the body do vary in density. These anatomical inhomogeneties cause x and gamma rays to be absorbed nonuniformly throughout the contour. It is therefore essential to have detailed density distribution within the contour in order to proceed with the isodose correction process so that the next level of accuracy can be achieved.

It has become increasingly more common to find dosimetry systems which allow the introduction of inhomogeneities within a contour. The input of these inhomogeneity data tends to be system dependent, most systems requiring the area to be sketched out on a visual display or entered on a digitizing surface. Some systems allow you to enter the density values for these regions, while others simply require you to identify them as lung or bone and then use preset density values for attenuation coefficients. When this procedure is examined, it can be seen that small errors in size and position of inhomogeneties, or in estimating their densities, can lead to errors as large as, or larger than, those which would have been encountered if no correction at all had been used. It can safely be stated that without the aid of inhomogeneity localization techniques and methods to measure the densities of these regions of interest, reasonable accuracy in these corrections cannot be achieved.

Many methods for positioning inhomogeneities have been used; orthogonal x-rays, transaxial tomography, computerized axial tomography, and ultrasound are among those most widely used. Of these, only computerized axial tomography can give the information required on position as well as density throughout all regions of the body. At first glance, the new generation of diagnostic scanners seems very well suited for the requirements of treatment planning, but a closer look shows that several disadvantages exist.

The first questions which must be asked are, what is the quantity which is being reconstructed by these scanners, and how can these data from a polychromatic beam operating in a photoelectric region be extrapolated with accuracy to attenuation coefficients for the supervoltage therapy, which is operating primarily in the Compton region? The second question concerns the actual treatment planning. If a local therapy department manages to obtain time to scan their patients on a local whole-body scanner, how will the remainder of the treatment planning procedure then be carried out? Either the raw data or reconstructed data would have to be transferred to a treatment-planning computer, or else the scanner's computer would have to be used for the treatment planning procedure.

Finally, there is the question of cost. Currently, a series of scans costs approximately $250 when performed in a diagnostic setting. If a therapy department were to obtain its own scanner, one which would see much less use than the one in a diagnostic setting, the cost per scan would then increase above these prices.

The object of this work was to design and build a whole-body scanner solely for the needs of radiation therapy. The criteria of overall low cost, simplicity of operation, and the ability to interface easily with

the department's existing systems have been used. Assuming that a therapy department capable of utilizing inhomogeneity data is likely to have either a dedicated treatment-planning computer of its own, or the use of a macro-computer via time-sharing, the scanner will not require the intelligence of a central processing unit. The system has therefore been designed around the hard-wired digital computer. This simple and low-cost computer, costing between $100 and $250, has the ability to control all scanning sequences with variable scan widths and variable angular shifts. The device also has the capability to start and stop all scanning motion through precise digital ramping sequences and to control all data collection.

To eliminate the problem of scaling data to the Compton region of interaction from the photoelectric region, cobalt-60 is evaluated as the source of the scanning beam. Since the reconstruction algorithms reconstruct to the linear attenuation coefficient of the energy being used to scan, the output of the reconstruction algorithm is then the value of the linear attenuation coefficient for cobalt-60 for each of our regions of interest. Because of the heavy, bulky shielding usually associated with cobalt-60 sources, a special collimator shield was required.

Both the collimator shield and detector are moved across the region of interest by stepping motors, gear reduction units, and precision ball screws. The width of the transverse scan and the number of degrees per angular rotation are variable from scan to scan. The transmission data are collected on a 3.3 millimeter grid, and the reconstruction performed on a one-quarter inch grid. Once the data have been recorded by a write-only tape recorder, the tape is transferred to the department's time-sharing computer.

The raw data are then reconstructed by an algorithm using filtered back projections. The proposed treatment planning algorithm utilizes these data to correct internal dose distributions.

In an effort to eliminate artifacts which would result from a standard treatment couch, a special two-section couch, which has longitudinal as well as vertical movement has been developed.

This paper documents the original design, assembly, and verification of an apparatus which, for the first time, makes accurate and reliable inhomogeneity data available to the radiotherapist.

CHAPTER 2

HISTORICAL DEVELOPMENT

Objectives

Until 1965, all isodose summation was done manually. This involved
the overlapping of isodose charts and adding up all intersecting isodose
lines. Because of the time involved in such a method, a specific set of
composite curves was not always compiled for each individual case. There
was therefore a need for improved dosimetry techniques and tools.

The practical goals for therapy put forth by Bloor and Quick
(1954) stated that, the aim of radiotherapy, in treatment of any
malignant growth, is the uniform irradiation of a minimum but adequate
volume of tissue to a dose that is likely to cause complete destruction
of the growth. In order to achieve these goals certain minimum
criteria must be met. These criteria are complete demonstration of
the depth dose distribution throughout the entire irradiated volume of
the patient so that, in particular, the inhomogeneity of dose within
the tumor may be judged, and that unnecessary radiation is avoided outside
the tumor bearing volume. Although these authors proposed new methods
for tabulating isodose data, their mothods still involved manual sum-
mation.

Methods of Internal Dose Corrections

Automation of Planning

It was a year later when Tsien (1955) stated that for system-
atic and reproducible therapy it would be essential to make up isodose
distributions for each particular treatment in planning a patient's
therapy. He was able to devise a coordinate scheme for calculating
doses within the radiation field with the criterion of limiting expo-
sures to all non-tumor tissue. Unfortunately, Tsien was limited by
the computational methods of the mid-fifties and thus employed punched
cards, a card sorter, and a tabulating machine. Once the data for each
patient had been transferred to punched cards, the automated method still
took 10-15 minutes to sort and tabulate the isodose values. By today's
standards, the method was very cumbersome and time-consuming; however,
it was the first large stride forward toward the automation of treat-
ment planning.

It was not until the 1960s that the next step was taken. Sterling
and Perry (1961) stated that one of the obstacles that had prevented
widespread application of automation was the difficulty of translating
the usual isodose graphs into numbers capable of being used by computing
machines. At this time, they proposed a method of digitizing the curves
manually into systematic grids. These grids were then fed into a
computer which summed the doses at various field combination points.
Because the state of "readily available" computers in 1961 was not
much more sophisticated than in 1955, computing by machine was still
a matter of summing data cards. Their method involved specifying doses
along every ten degrees of the field. This involved 36 cards per field.
The problems associated with card storage and manipulation for the

minimum number of fields needed for routine work can easily explain why, at this point in time, not everyone was willing to automate.

The impracticality of storing field data on punched cards was realized by Siler and Laughlin (1962) who estimated that a minimum library necessary to achieve a reasonable level of accuracy was 3,000,000 punched cards. They decided to abandon storing data on cards and go to an alternate system of equations which would, in place of cards, specify the radiation field. Their method used tissue-to-air ratios (TAR), off-center ratios (OCR), and an inverse square correction as field parameters. They felt that inhomogeneities should be considered in the field corrections. To achieve this correction, they expressed the TAR as a function of electron density and tissue thickness. Although the authors were correct in attempting to take into account inhomogeneities, they posed no method for locating them.

Through the next several years of development, many methods of computing radiation fields within the body were developed. (Skaggs and Savic (1962), Sterling, Perry, and Katz (1963), Bentley and Inst (1963) and Hallden, Ragnhult and Roos (1963) were but a few of the more prominent researchers of this era.) It was not, however, until 1965 that a completely automated method of treatment planning with auto-mated output plotting of isodose curves within the body cross section for rotational therapy was developed by Mauderli and Fitzgerald (1965). Although the method reported employed manually digitized isodose curves, a method of acquiring the isodose field data in digital form by the direct measurement of the radiation field had been proposed and de-veloped (Mauderli and Hazard, 1965). It was also in 1965 that Sterling, Perry and Weinkam developed a method of calculating and displaying the total treatment volume by a series of two dimensional projections at different depths through the area of treatment.

Inhomogeneity Corrections

At this time, the accuracy of treatment calculations were limited by the lack of one important set of patient parameters: the coordinates positioning the actual inhomogeneities within the body. Setala (1965) addressed this problem and developed a method of internal organ localization based upon views in two orthogonal x-rays. The positions of inhomogeneities were transferred to a "contour equivalent" of the patient and the data then hand digitized for computer use. The problems encountered with slight movements of the patients between x-rays and contour mapping lead to inaccuracies which limited the use of the method.

The first attempt to accurately compensate for inhomogeneities was by Eichorn (1967). Eichorn built a phantom of the thorax in which he placed inhomogeneities that simulated bones and lungs. Knowing the actual position of the internal structures and their x-ray attenuation properties, calculations were made. The phantom was equipped with measuring sites and thermoluminescent dosimeters, TLDs were used to measure the dose for a simulated treatment. The good agreement between the calculated and measured values demonstrated the ability to calculate actual isodose values given the necessary information on internal structure and attenuation coefficient.

The increase in knowledge of isodose fields, computer treatment planning, and isodose contour displays since 1967 have all added to the speed and accuracy with which the routine treatment plan can be executed. Unfortunately, the accuracy and speed are still limited to two factors: (1) accurate contour measurement and (2) correction for inhomogeneities.

Computerized Axial Tomography

The largest strides in solving the problem of inhomogeneity defi-
nition has been in the development of axial tomography. This technique,
first developed into a useful clinical tool by Hounsfield (1973) in
1969, yields the positioning of anatomical inhomogeneities via a map
of relative radiation attenuation numbers. His first unit was dedicated
to examination of the head. However, by the time a marketable machine
was announced in 1972, the development of a similar unit capable of
rendering tomographs of any section of the body was announced by
Ledley, et al. (1974). Since 1972, nearly 40 companies have proposed
production of axial tomographic scanners.

The availability of axial tomographic devices which scan with
x-ray beams of energies ranging from approximately 80 to 140 Kv have
attracted significant scientific interest. The numbers which these
units obtain, as solutions to their reconstructive algorithms, show
promise in their ability to correlate with electron densities of the
material being scanned. The work by Phelps et al. (1975) demonstrates
the relationship between the computerized tomography, CT, numbers, and
the electron density of materials such as Teflon, Bakelete, Plexiglas,
nylon, and water. The fact that one material at a time was scanned
is of interest. McCullough, (1976), disputes the ability of CT scanners
to achieve a resolution of 1.5% in the "quantity" that is being recon-
structed. He alludes to a resolution in excess of 2%. This error would
only be the first error in the calculation for the attenuation coef-
ficient needed for therapy. Since a large number of therapeutic
treatments are performed with energies ranging from that of cobalt-60
(1.17 and 1.33 MeV) on up to energies including and beyond 20 MeV,
a second calculation would have to be made in order to scale the data
to the attenuation values applicable for supervoltage therapy.

The type of procedure currently in practice is similar to that explained by Jelden, et al. (1976), and usually involves several steps. The CT scan must be taken and the image must be transferred from the scanner into the treatment planning computer. Some companies, realizing the applicability of this data to radiation therapy, are designing computer systems which will support a computerized axial tomographic CAT scanner and also support a therapy's department treatment planning requirements. Once the data transfer has been accomplished, a density plot is calculated. This is done by the bracketing of CT numbers into several discrete levels. For example, a simple algorithm assigning areas as tissue or muscle equivalent, soft bone or cartilage equivalent and dense bone equivalent might be used. The scale which might typically be available on a CT scanner may range, depending upon the unit, from -500, the value for air, to +500, the value for reconstructed dense bone, with water being at 0. This scale can lend itself to many density ranges but usually three to five are sufficient. The data are then used by a treatment planning program which is sensitive to density data.

An alternative to the normal x-ray CT scanner is a cobalt-60 CT scanner. This type of scanner has several advantages over presently available x-ray scanners. One of the main advantages is that the monochromatic beam enables the reconstructive algorithm to reconstruct each image element to the linear attenuation coefficient for cobalt-60. A second advantage is that since very fast scan times are not necessary, and a constant intensity isotope has replaced the x-ray source, the overall design of the apparatus can be simplified. Thirdly, since most therapy departments have treatment planning computers, these same computers can be used for the reconstruction of the new data and a simple low cost scanner, one which can be afforded by a therapy department, can be fabricated.

Cobalt-60 scanning systems have been proposed by Thieme, et al. (1975) and Hendee, et al., (1976). However, a clinically useable system has yet to be announced.

A functional design for a high energy scanner is not as obvious as is its need. The problems associated with the shielding of a high energy isotope complicates the design of both the mechanical and the electronic systems. The final design presented, is the result of many trial and error design procedures and fulfills the requirements of reliability, precision and low cost.

CHAPTER 3

RECONSTRUCTIVE METHODS

The basic principle on which axial tomographic scanners are based
involves the taking of multiple transmission measurements through an
object and then reconstructing these measurements into an image free of
interference from overlapping material.

The method of imaging internal structure without the interference
of overlapping material has been a long standing problem in many
disciplines of science. Unfortunately, the interdisciplinary communi-
cation of the scientific community is often very poor. Only after an
advance significant enough to receive wide publicity was the fundamental
applicability of many independent works realized and classified under
the common heading of reconstruction of images from their projections.

Tomography

One of the first attempts to solve the internal imaging problems
was known as tomography. The early tomograms were performed by the
relative movement of an x-ray source, and recording film was synchronized
so that only one sagittal plane within the body remained fixed relative
to the imaging equipment. All the other planes, through which the x-ray
must pass, would experience relative movement and therefore, the images
would experience fogging. The resulting image would be that of one

focused plane superimposed on a background of blurred planes. This type of tomography was known originally as planigraphy (Andrews, 1935) and later as focal plane tomography. Focal plane tomography remained the only type of tomography available to the medical community for over forty years.

From 1956 to 1972 the advances which eventually lead to the present-day tomography units were taken in the fields of radioastronomy and electronmicroscopy. These efforts were, for the most part, independent and only after the large interest generated by diagnostic tomographic scanners introduced in 1972, were the isolated works categorized under the general heading of Reconstruction from Projections.

Reconstruction from Projections

History

The first step towards a reconstructive image was taken in radio-astronomy by Bracewell (1956). He faced the problem of obtaining a microwave image of the surface of the sun with a radiotelescope which could only focus on strips across the entire surface of the star. The microwave signal would therefore be the summation of all the signals emitted in a two dimensional rectangle. Bracewell proposed that these strips be "reconstructed" into an image of the entire surface by a method utilizing Fourier transforms, but in 1956 the state of the art in computer science made the computation of an inverse two dimensional Fourier transform an insurmountable task. He was therefore forced to resort to a technique known as iterative reconstruction.

Twelve years after Bracewell's publication the problem was being solved again in the field of electronmicroscopy (Morgan, 1968; DeRosier and Klug, 1968). The problem was to obtain a cross section of an object which could only be viewed by a transmission electron beam. This problem was analagous to Bracewell's in that only the integral value of the strip could be obtained. In the twelve years that lapsed since Bracewell's reconstructive attempts, the field of computer science had advanced to the point where the implementation of inverse two dimensional Fourier transforms was now applicable.

Aside from these two advances, there were literally dozens of articles published on the topic in both fields with variation in reconstructive methods as well as data acquisition being reported. The review article of Brooks and DiChiro (1976) details the history and put the various reconstructive approaches in perspective.

The applicability of reconstructive tomography was not introduced to the medical community until EMI Limited introduced their axial tomographic scanner in 1973, (Hounsfield, 1973).

The EMI scanner collected transmission data of a patient's head. These transmission measurements were again a summation of the partial transmission of many single elements, similar to the data obtained in electronmicroscopy. In this original unit, the reconstructive approach was known as the Arithmetic Reconstruction Technique.

The valuable information which the EMI scanner made available to the medical community generated an interest in not only the apparatus used, but the mathematical techniques employed. It was at this time that attention to the applicability of the independent works were viewed under the common heading of reconstruction from projection, and in the medical field more specifically, reconstructive tomography.

Nomenclature

Before various methods of reconstructing cross sections from their projections are explained, the nomenclature and methodology of the projections should be discussed. Let the object O in Figure 3.1 be the object to be scanned and reconstructed.

Sitting on opposite sides of the object O are the Detector D and the source S. The source emits a beam; in the case of the cobalt-60 scanner, the beam is composed of the gamma radiation of a ten Ci cobalt-60 pellet. The detector measures the transmitted portion of the radiation beam; this portion will be denoted as P. The gamma-ray beam in Figure 3.1 is at a distance r from the origin and makes an angle $\emptyset$ with the ordinate. If the path length of the ray is s, then P, the partial transmission of the beam, is given as P $(r,\emptyset)$ and is equal to the transmission of the ray through path s or

$$P(r,\emptyset) = \int_{r,\emptyset} f(x,y)ds \qquad 3.1$$

where $r = (y)$sine

and $f(x,y)$ is the function which describes the attenuation of beam. In the case of the monoenergetic beam of radiation

$$I = I_o exp[\int_S -\mu(x,y)ds] \qquad 3.2$$

where: I_o is the initial unattenuated beam intensity at the detector

I is the intensity of the beam after it has traversed path s.

$\mu(x,y)$ is the linear attenuation coefficient for the radiation being used.
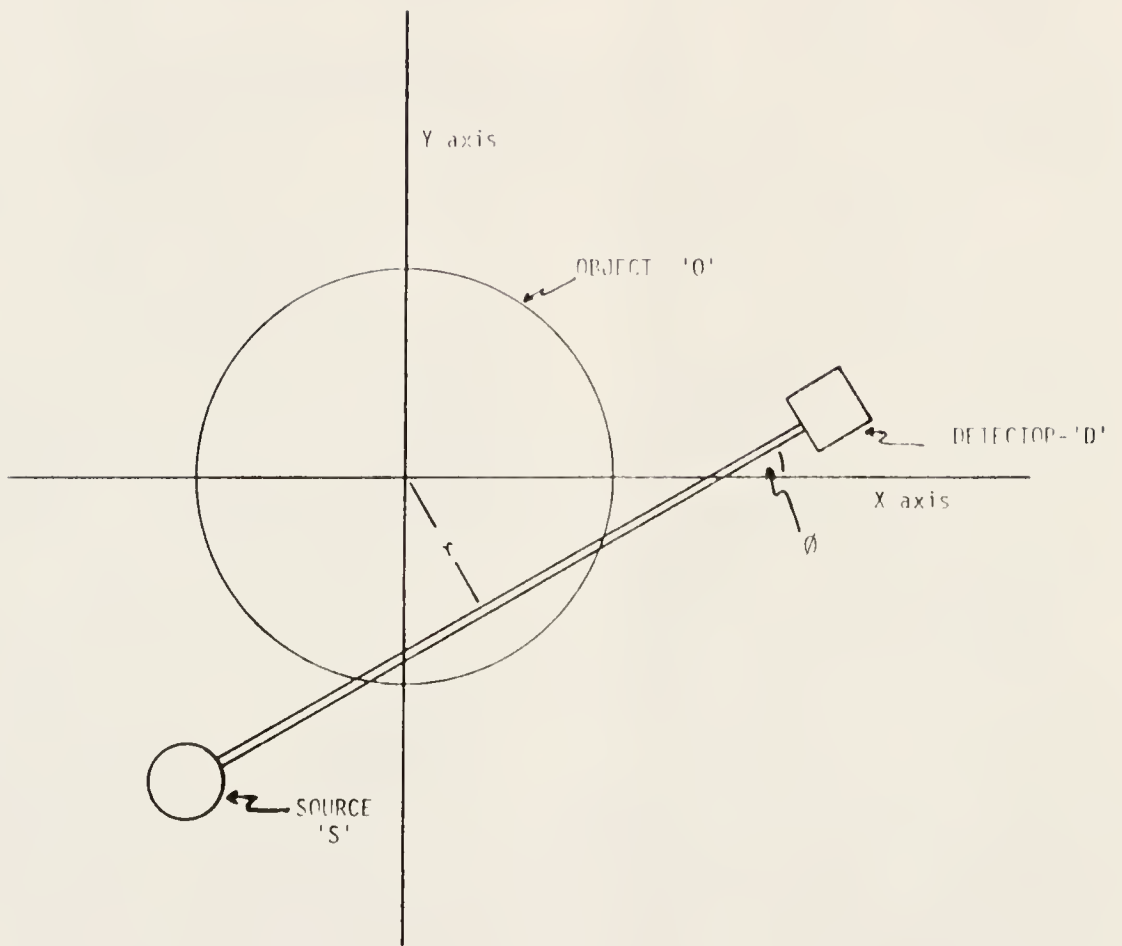
If the transmission is defined as

Figure 3.1. Scanning Geometry.

$$P' = \ln(I/I_o)$$

then Ez. 3.1 can be rewritten as

$$P'(r,\emptyset) = \ln \frac{I(x,y)}{I_o(x,y)} \qquad 3.3$$

During the scanning procedure the object being scanned is
confined to a space of diameter d. The data is collected and the
reconstruction performed at spacing of the ray width a. The
number of points in any scan pass at an angle $\emptyset$ will be $N=d/a$ and
the total number of reconstructed points will be N. Each of these
points will henceforth be referred to as picture elements (pixels).

After N measurements are made at angle $\emptyset$, the source and detector
rotate $\Delta\emptyset$ about the origin and another set of N values is obtained.
This procedure is continued until K sets have been measured, where

$$K = (\pi/\Delta\emptyset) \qquad 3.4$$

The scanning is stopped at this point because

$$P'(r,\emptyset) = P'(r,\emptyset + \pi) \qquad 3.5$$

thus all further data collection would therefore be redundant.

After the $P'(r,\emptyset)$ array has been determined, the data collection
is complete. The reconstruction techniques therefore has knowledge of
the coordinate system, the scanning sequence, and the N·K values of
transmission data in the two dimensional $P'(r,\emptyset)$ array from which it
must reconstruct the object.

In the following discussion on reconstructive techniques, it will be assumed that the measurement and recording of transmission data is performed without distortion or alteration of the data. It will therefore be assumed that any distortions or artifacts in the final image are due to either the scanning procedure or the reconstructive technique.

Equation 3.2 shows that the scanned data, or transmission data, is dependent upon only one quantity, namely $\mu(x,y)$. Most reconstructive techniques will therefore attempt to yield a quantity which can be correlated to the linear attenuation coefficient.

Numerical Reconstructive Tomography Methods

Back Projection

This method was used by Oldendorf (1961) for the first experiments in reconstructive tomography. In this technique, the data taken at each angular orientation, $\emptyset$, are projected back to a common space. Each transmission value at a particular angle, $P(r,\emptyset)$, is projected back on, or added to, each pixel along the ray path s through which it was measured. The magnitude of each pixel is therefore the summation of all transmission rays which pass through it. Although the image is an overestimation of the original object, it will have merit as a qualitative representation. The advantage of this method is that it can be implemented without the aid of a computer, although the quality of the reconstruction generally is poor.

The effect of projecting the ray value to each pixel which contributes to the ray can be seen in the region of abrupt inhomogeneities.

This produces a star pattern around the inhomogeneity with the number of points on the star being equal to the number of views, K.

Iterative Techniques

The object of the iterative techniques, unlike that of the Back Projections, is to ascertain the correct value of (x,y), the linear attenuation coefficient, for each of the N pixels.

The technique obtains, through various procedures, a matrix of N linear attenuation coefficients. Transmission data are calculated using these values and then they are compared to the measured data. The values of the attenuation coefficients are altered to obtain a better agreement between the measured and calculated data sets. This procedure is continued until all N pixels have been adjusted. If the overall fit of the calculated transmission rays to the measured transmission rays is not within a preset tolerance, the procedure is reiterated until the error between the calculated and measured transmission data is within acceptable limits.

Iterative Least Squares Technique

The Iterative Least Squares technique performs the above procedure by calculating the entire transmission matrix and then calculating the corrections for each element of the attenuation matrix. The correction of all pixels are made after which another calculated scan is performed. This procedure is repeated until the error between calculated and measured data is within a preset limit.

All of the attenuation coefficients being updated at the same time causes this method to over correct the pixels. This occurs because a pixel with a value lower than the corresponding image point will be

corrected from all K views before it is re-evaluated. To impede the size of the correction the best-least-square fit to the measured data is used to decide upon the degree of dampening required. Because of this criteria, this technique has been termed the Iterative Least Square technique (ILST).

Simultaneous Iterative Reconstruction Technique

An alternative method of adjusting the linear attenuation coefficient is to alter the values point by point. In this method, all of the transmission rays which pass through a single pixel are calculated. That pixel's value is adjusted and the next pixel is then considered. After all N pixels have been adjusted, the overall closeness of calculated to measured data is examined. If the two differ by too large an amount, the process is reiterated. Because this method corrects the pixel simultaneously with the calculation of all transmission rays through it, it has been termed the Simultaneous Iterative Reconstructive technique (SIRT).

Algebraic Reconstructive Technique

The third technique calculates the transmission data for a particular angular orientation. It then corrects the attenuation coefficient and goes on to another orientation. If the calculated values do not agree to within a specified tolerance with the measured data, the procedure is reiterated. This procedure has been termed the Algebraic Reconstruction technique (ART).

Of these techniques, the ART will converge most rapidly at first, but has problems with noisy data where as the ILST and SIRT do not converge as rapidly, but are better able to handle noisy data. As proposed by Brooks and DiChiro (1976, pg. 707):

an optimum iterative procedure may be one that uses ART
for the first one or two iterations and switches to ILST.

These authors chose the ILST over the SIRT because of the shorter
computational time per iteration.

Analytical Reconstructive Tomography Methods

The Fourier Transform Method

A second approach to reconstructing the raw data is to use analy-
tical methods. One such method involves the use of Fourier Transforms.
This method is explained by Gordon and Herman (1970, pg. 113):

> The Fourier method depends on transforming the projec-
> tions into Fourier space, where they define part of the
> Fourier transform of the whole object. Each projection
> may be shown to yield values on a central section of
> Fourier space, which is a line or plane (corresponding
> to the two or three dimensional problem) through the
> origin at an angle corresponding to the direction of the
> projection in real space. An attempt is then made to
> interpolate the unknown values of the full Fourier trans-
> form from the values of the central sections. After
> interpolation a reverse Fourier transform provides an
> estimate of the object's structure.

In this method, the raw transmission data are obtained in the scan-
ning sequence previously explained. If we represent the transmission
data of a particular view by a continuous function P with a period d,
where d represents the scan width, then the function $P(\emptyset)$ is a one dimen-
sional projection of the data at a particular angle $\emptyset$. The following
development follows closely that of Gordon and Herman (1970).

If we allow $F_1P_\emptyset$ to be the Fourier Transform of this projection then for any R

$$[F_1P_\emptyset](R) = \int_{-\infty}^{+\infty} \exp[-2\pi jR\mu] \cdot [P\emptyset](\mu)d\mu \qquad 3.6$$

This now represents the line projection of the central section of the object. The Fourier Transform of a two variable function, for example, the two-dimensional surface of the image, is defined as

$$[F_2f](X,Y) = \int_{-\infty}^{+\infty}\int_{-\infty}^{+\infty} f(x,y)\exp[2\pi j(X,Y)]dxdy \qquad 3.7$$

where in this case f(x,y) represents the two-dimensional linear attenuation coefficient. The inverse two-dimensional transform is defined as

$$f(x,y) = \int_{-\infty}^{+\infty}\int_{-\infty}^{+\infty} [F_2f](x,y)\exp[-2\pi j(X,Y)]dXdY \qquad 3.8$$

Equation 3.8 demonstrates that if $[F_2,f]$ (x,y) is known, the f(x,y) can be ascertained.

Let S be the operator that maps a two-dimensional function onto a one variable function by restricting it to a line through the origin. Then for R, which measures the distance along the central section of the projected object

$$[S_\emptyset F_2f] = [F_2f](Rcos\emptyset,Rsin\emptyset). \qquad 3.9$$

Since P has already projected f(x,y) to a line through the central section

$$[S_{\emptyset}F_2 f] = [F_1 P_{\emptyset}](R),$$ 3.10

and, by substituting Eq. 3.10 into Eq. 3.9,

$$[F_2 f](R\cos\emptyset, R\sin\emptyset) = [F_1 P_{\emptyset}](R)$$ 3.11

This demonstrates that the two dimensional Fourier Transform $F(x,y)$ can be obtained by the use of the original transmission data, $P(r,\emptyset)$.

Because the reconstruction matrix is a rectangular coordinate system and the scanning procedure employs a polar coordinate system, the data at a specific point (x,y) may not be available. This means an interpolation in two dimensional Fourier space must be performed. If any interpolating scheme, more complex then a simple linear fit, is used, this interpolation time dominates the overall computation time of the method.

The Convolution Method

In order to eliminate the two dimensional Fourier space interpolation and to decrease the total computational time, an alternate method was developed. The following developments follow closely that of Ramachandran and Lakshminarayanan (1971).

Their method employs the well known convolution theroem. Given two functions $f(x)$ and $g(x)$ and their Fourier transforms $F(t)$ and $G(t)$, respectfully, then:

$$f \star g \equiv \frac{1}{2\pi} \int_{-\infty}^{+\infty} g(y)f(x-y)dy$$ 3.12

is defined as the convolution, or as also called the Faltung, which is

the German term for folding, of function f(x) and g(x). As shown by Arfken (1966)

$$\int_{-\infty}^{+\infty} F(t)G(t)\exp(-itx)dt = \int_{-\infty}^{+\infty} f(x-y)g(y)dy. \qquad 3.13$$

The Fourier inverse of a product of Fourier transforms is the convolution of the original function.

If Eq. 3.8 is rewritten in polar form:

$$f(r,\emptyset) = \int_{0}^{2\pi} \int_{-\infty}^{+\infty} F(R,\theta)\exp[-2\pi iRr\cos(\emptyset-\theta)]RdRd\theta \qquad 3.14$$

where $\emptyset$ is the angular orientation of the reconstruction grid, and the orientation of the data acquisition system. This can be rewritten as

$$f(r,\emptyset) = \int_{0}^{\pi} \int_{-\infty}^{+\infty} |R|F(R,\theta)\exp[-2\pi iRr\cos(\emptyset-\theta)]dRd\theta. \qquad 3.15$$

If $P'(\ell, \theta)$ is defined as

$$P'(\ell,\theta) = \int_{-\infty}^{+\infty} |R|F(R,\theta)\exp[-2\pi iR\ell]dR, \qquad 3.16$$

then by substitution

$$f(r,\emptyset) = \int_{0}^{\pi} P'(r\cos(\emptyset-\theta),\theta)d\theta; \qquad 3.17$$

changing Eq. 3.17 into polar form

$$F(R,\theta) = \int_{-\infty}^{+\infty} P(\ell,\theta)\exp(2\pi iR\ell)d\ell, \qquad 3.18$$

and Fourier inversion yields

$$P(\ell,\theta) = \int_{-\infty}^{+\infty} F(R,\theta)\exp[-2\pi R\ell]dR. \qquad\qquad 3.19$$

It can now be shown that the Fourier transform of $P'(\ell,\theta)$ equals the Fourier transform of $P(\ell,\theta)$ times the Fourier transform of $g(\ell)$ where

$$|R| = \int_{-\infty}^{+\infty} q(\ell)\exp[2\pi iR\ell]d\ell \qquad\qquad 3.20$$

using the definition of the convolution

$$P'(\ell,\theta) = \int_{-\infty}^{+\infty} P(\ell,\theta)q(\ell-\ell_1)d\ell_1 \qquad\qquad 3.21$$

Since $P(\ell,\theta)$ is the transmission data, which are known, if $g(\ell)$ can be obtained then using Eq. 3.17 one can obtain the attenuation coefficient matrix.

Fourier inversion of Eq. 3.20 yields

$$q(\ell) = \int_{-\infty}^{+\infty} |R|\exp(-2\pi R\ell)dR. \qquad\qquad 3.22$$

It can be seen that this equation can not be evaluated because of the divergence of the integral. If the limits $-\infty$ to $+\infty$ are replaced by $-A/2$ and $+A/2$ where A is a very large finite number, Eq. 3.22 can be written as

$$q(\ell) = \int_{-A/2}^{+A/2} |R|\exp[-2\pi iR\ell]dR. \qquad\qquad 3.23$$

If ℓ is replaced by na where a is the ray width from Eq. 3.22 and n is an integer, the solution to Eq. 3.23 can be shown to reduce to:

$$q(na) = 1/4a^2 \text{ for } n=0$$

$$q(na) = 1/(\pi n)^2 a^2 \text{ for } n=\text{odd}$$

$$q(na) = 0 \text{ for } n=\text{even}$$

Eq. 3.2 can now be rewritten using $\ell = ma$:

$$P'(na,\theta) = a \sum_{m=-\infty}^{+\infty} P(ma,\theta)q((m-n)a) \qquad 3.24$$

where m is a positive or negative integer.

Eq. 3.24 yields a set of filtered or weighted transmission values. Eq. 3.17 can now be used to backproject these values to the common space $f(\ell,\theta)$. Because the sampling of the data occurs at a regular spacing and the angular shifts also are performed along regular angular intervals, Eq. 3.17 in discrete form is:

$$f(jr_0,\theta_0) = \theta_0 \sum_{t=1}^{k} P'((jr_0\cos(k\emptyset_0-t\theta_0),t\theta_0) \qquad 3.25$$

where: t, j, and k are integers and r_0 and θ_0 are the spacings of r and θ. As can be readily seen

$$jr_0\cos(k\emptyset_0-t\theta_0)$$

will generally not be a multiple value of "a". Thus, the required value must, therefore, be interpolated, but in real space, not Fourier space, and in only one dimension.

CHAPTER 4

MECHANICAL DESIGN

Design Criteria

The transmission of ray $P(r,\emptyset)$, of Equation 3.1 denotes the trans-
mission of a photon beam through a group of pixels. The equations used
in the reconstructive process assume theoretically ideal movement of
both transverse and rotational systems. The precision required during
data acquisition can be brought into perspective by examining a single
pixel size and comparing it to the total distance traversed during the
scanning process. The entire distance traversed during the scanning
of a 40 centimeter by 40 centimeter grid with 36 angular shifts is
over 14 meters, neglecting rotational movement. When one considers
that each pixel is less than one-thousandth of that distance, the
strict requirements placed upon the mechanical system can be appreciated.

Most first generation scanners, those with moving source and
moving detectors, fixed the source and detector to a hollow yoke which
is traversed and rotated around the patient. While these first gene-
ration scanners were being designed, the basic design for the cobalt-60
system presented in this work,was taking place. It was decided to
utilize a design which uses ball screws for the traverse movement and a
large drum to facilitate rotation. Anticipated problems in this design
were:

(1) loss of accuracy when the screw is reversed

(2) misalignment of detector and source due to variation in the
screw lead

(3) isocentric inaccuracy due to a nonuniform surface of the
rotating drum, and

(4) maintaining rigidity of the unit to withstand the changing
forces as the detector and collimator traverse.

Some of these problems are more difficult when dealing with a cobalt-60
scanner than with a conventional x-ray scanner, due to the addition of
several hundred pounds of special materials which are required for
shielding and collimation of the radiation beam.

In order to determine the consequence of these potential problems,
a detailed examination of the system must be made.

The equation for the nth transmission ray at angle $\emptyset$ is:

$$Y = (-x)\tan(\emptyset + \Delta\varepsilon_1) + (n-n_1)(a + \Delta\varepsilon_2)\tan(\emptyset + \Delta\varepsilon_1),$$

where the error due to drum misalignment and rotational inaccuracy is
given by $\Delta\varepsilon_1$ and the error due to inaccuracies in the traverse mecha-
nism is given by $\Delta\varepsilon_2$. Since the scanner utilizes rotation as well as
the traverse motion, these errors can be either positive or negative.
For example, if the scanner is in the orientation shown in Figure 4.1,
the load on the drum will cause an error resulting from the flexing or
looseness in the rotational mechanism, in the counterclockwise direction,
while when in the orientation of Figure 4.2, just one traverse later,
the error will be in the clockwise direction. Errors can also be
expected whenever the direction of the driving forces change as is
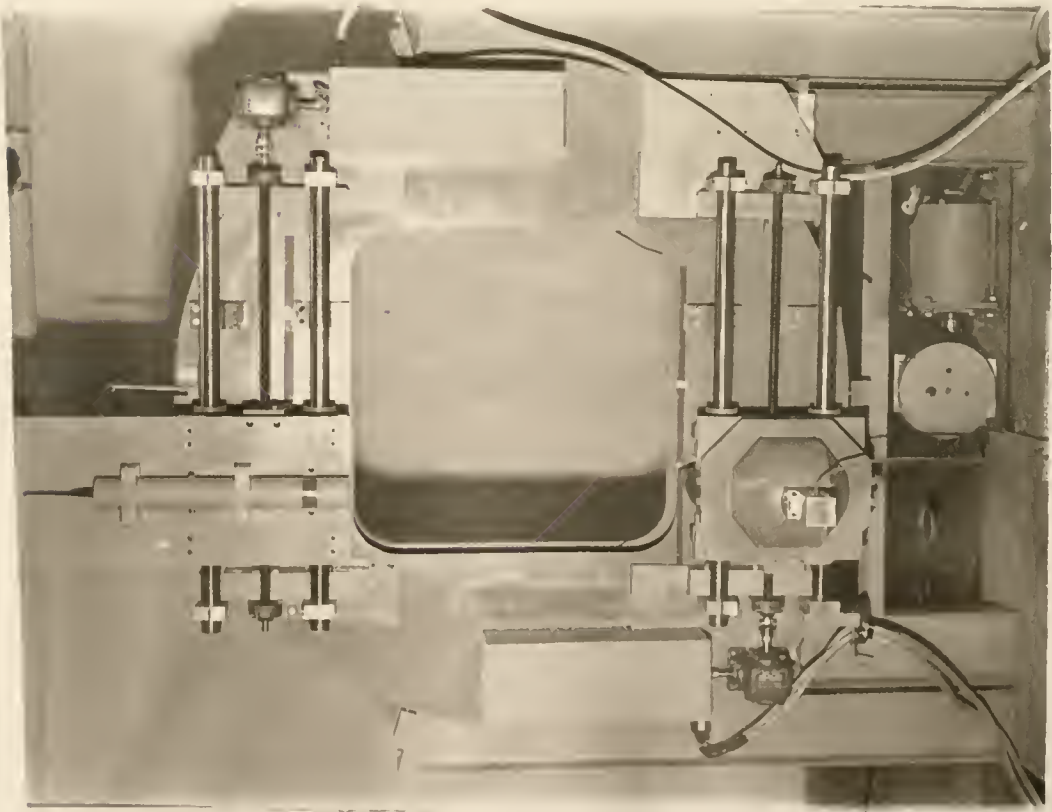experienced in alternate traverses. While the lead of the screw will

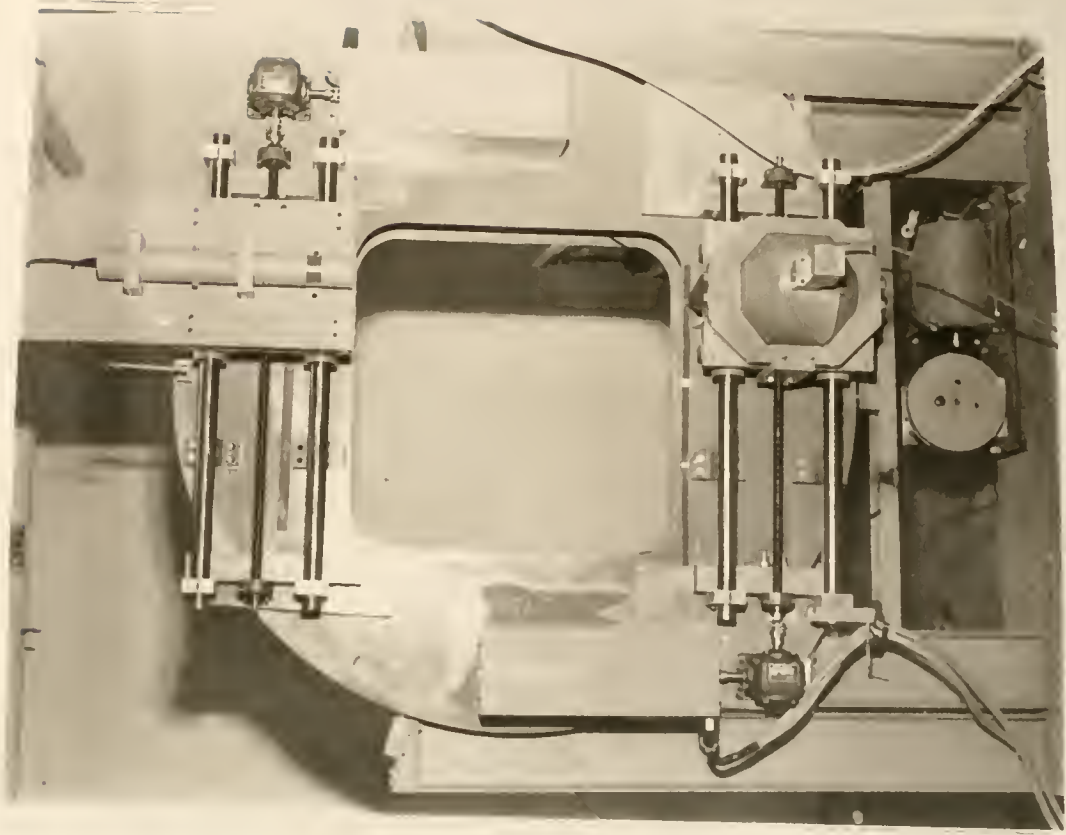Figure 4.2. Diagram showing the forces which result in a clockwise error.

Figure 4.1. Diagram showing the forces which result in a counter-clockwise error.

have a negative or positive error, the backlash of the ball nut will give an error in the direction of the prior traverse when the screw is horizontal, or in the direction of gravitational forces when the screw has a force component opposing gravitational forces.

Mechanical System

The final scanner design has resolved these and other problems and reduced the errors to acceptable limits. The inaccuracies in the rotational center were minimized by machining the surface of the rotational drum to within 0.005 inches of round over its 54 inch diameter. It was also decided to use a metal drum supported by bare metal bearings to eliminate any problems due to a padded surface flexing under load. In the original design, the drum was to be driven through the use of a chain, but when the small play in each link was totaled over the seven feet of chain required to span the drum and drive the pulley, the overall error would allow the drum to rotate several degrees during the shifting load situations of Figures 4.1 and 4.2. This problem was solved by the use of a nylon core rubber belt which could be loaded so that undesirable rotational shifts were eliminated. The drive system for the drum consists of the above mentioned drive belt, a 10:1 gear reduction unit, and a DC stepping motor, SLOSYN Model No. SS1800-1007, which steps in 1.8 degree increments. The design of the motor is such that the error per step is noncumulative and has a maximum error of plus or minus 3% of one step.

The traverse system has also been made rigid through several design specifications. Ball screws are normally designed to withstand much greater axial than transaxial loading, therefore 1-1/2 inch hardened

steel shafts have been used to support the load transaxially. To elimi-
nate the backlash double ball nuts were used with preloading to an
excess of 300 pounds. The stepping motors used, WARNER Motor No. SM-
024-0140-FB, which step in 15 degree increments, are accurate to within
plus or minus 5% of one step and, as with the SLOSYN motor, the error is
noncumulative.

The ball screws are driven by a 10:1 gear reduction unit
which is driven by one or more DC stepping motors. In the original
design one stepping motor was used to control the source and one to con-
trol the detector. The calculated and measured torque are within the
rated range of the stepping motors, when stepping at a speed of about
720 steps per second. The original gear reduction was to be 10:1
which would move the source and detector at a speed of four centimeters
per second. Unfortunately, the stepping motors could not be made to
step at this speed while under the required load. The first attempted
solution employed ramping sequences to bring the motors up to speed in
several steps, but after considerable effort it was finally decided
that the step rate of 720 steps per second would have to be temporarily
abandoned. In an effort to increase the available torque, two motors
were placed in series to drive the source. Viscus dampers on both source
and detector were used to avoid resonance, a problem which stepping
motors can experience while slewing. The maximum speed which could be
reliably obtained was 300 steps per second. There was still, however,
the problem of being sure that the motors followed the pulse sequence
sent to them, this was especially a problem at the beginning and end of
a traverse. Through experimentation it was found that if an eight step
digital ramping sequence was used for acceleration as well as deceleration
no steps would be lost, even under the worst load conditions. This
circuit will be discussed later.

This final design has several advantages over those normally used in axial tomographic units. Since no signal is required to be sent back from the mechanics, the driving electronics could be simplified. A constant traverse speed allows the measurement of transmission data by the method of repetitive intervals (Fitzgerald - 1974). This method requires that the integration over a specified time interval be equal to the integration of the signal over a specified distance. If either DC or AC motors are used in such a changing load situation and the electronics relies on positional pulses from the mechanical system to initiate or terminate integration intervals, a large variation in integration time could be experienced.

Patient Support System

In order to support the object to be scanned, a couch was required. The couch should fulfill the criteria of minimal perturbation of the scanning beam while allowing the patient to lie in a position similar to that used during treatment. This system, fabricated in two independent sections and joined by a two-inch thick, eight foot long, slab of styrofoam, allowed the object to be scanned with only the styrofoam in the plane of the scanning beam. In order to eliminate any beam perturbation due to the styrofoam, the couch was placed in the scanning position during collection of data used to formulate the correction matrix, a procedure which will be discussed later. The algorithm which corrects for system misalignments would then simultaneously correct for any artifacts produced by the couch.

Radiation Source

The cobalt-60 beam has several criteria involving collimation and intensity which in turn dictate design restrictions for both the source and its collimator shield housing as well as the collimator for the detector. When looking at the intensity required for the source the first criteria which should be investigated is the statistical fluctuations per counting interval. It is desirable for each interval to have a measured pulse rate accurate to within plus or minus 1%. In order to guarantee this accuracy, a pulse rate of 10,000 pulses per interval must be set as the lowest pulse rate obtainable. During the initial design, it was decided to collect data at 0.5 centimeter intervals while traversing at a speed of four centimeters per second. This translates into a minimum pulse rate of 80,000 pulses per second. The conditions under which the minimum count exists should be that of maximum patient thickness. Assuming that the worst case is that of 45 centimeters of tissue attenuating the beam, only 8% of the initial beam would be available for counting. The full intensity of the unattenuated beam, in the worst case, would need to be 12.5 times more intense than the 80,000 pulses per second minimum. Thus 10^6 is the number of pulses which must be detected when the beam passes through an area which lacks any attenuating material other than air. The actual intensity of the beam would be such that when multiplied by the efficiency of the detector 10^6 counts per second are detected.

Radiation Detection

When the detection efficiencies of various scintillators were examined, Sodium Iodide (thallium activated), NaI(Tl), was chosen as the

best suited for this particular application. Although the response
time of NaI(Tl) is not exceedingly fast, when compared to other detec-
tors, its high detection efficiency makes a large enough difference in
source strength, and therefore source shielding, to outweigh this slow
response. A NaI(Tl) crystal 1.9 centimeters in diameter and 10.16
centimeters long was fabricated by Harshaw Chemical Company, and coupled
to a 0.75 inch photomultiplier tube. The crystal and photomultiplier
assembly was hermetically sealed inside a stainless steel cylinder in
such a way that the photomultiplier was insulated from the walls so
that is could be used with either positive or negative high voltage.
For pulse rates above approximately 0.8×10^6 pulses per second NaI(Tl)
cannot be used in the pulse mode, but instead must be used in the cur-
rent mode. This is advantageous because the detection efficiency for
NaI(Tl) in the current mode is much larger than in the pulse mode. The
above detector has an efficiency of over 85%. Therefore, the total
number of photons per second reaching the detector must be approximately
1.2×10^6 for an effective detection rate of 10^6.

Radiation Beam Collimation

The fact that pulse counting will not actually take place does not
alter the fact that the minimum pulse rate mentioned will be required
to assure that there be less than 1% fluctuation of detectable radiation.
It is not possible to perform pulse height and analysis when NaI(Tl) is
used in a current mode, therefore scattered radiation cannot be distin-
guished and is thus counted as primary contribution. This problem can
be greatly reduced by placing rigid restrictions on the collimation of
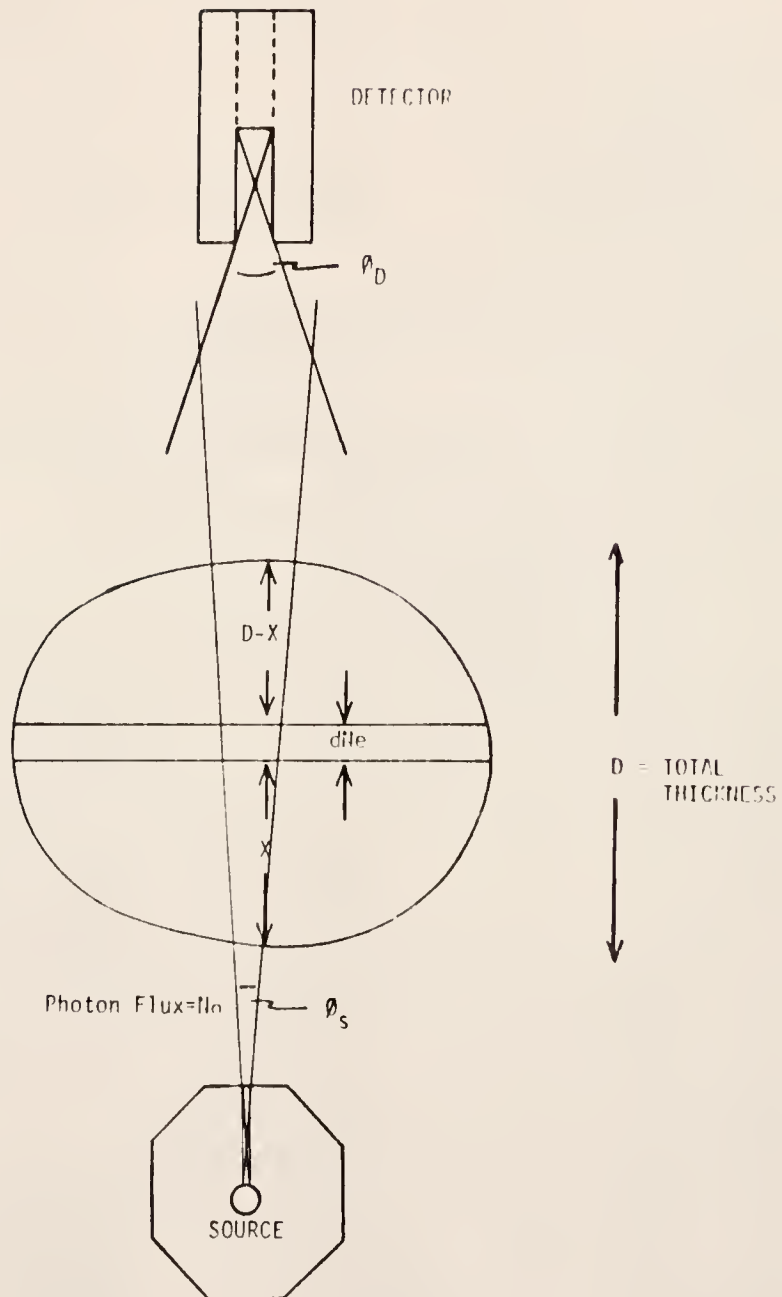both source and detector. Figure 4.3 shows the relative positions of

Figure 4.3. Source Detector Geometry.

the radiation beam and detector during scanning. The tangent of the angle, $\emptyset_s$, at which the radiation leaves the source collimator is defined as the diameter of the collimator over its length:

$$\emptyset_s = \tan^{-1}\left[\frac{\text{diameter of source collimation}}{\text{length of source collimation}}\right].$$

In the cobalt-60 scanner, the source collimator was designed with a portal that is 1.98 millimeters in diameter and 102 millimeters long. The angle $\emptyset_s$ is therefore

$$\emptyset_s = \tan^{-1}\left[\frac{D}{L}\right] = \tan^{-1}\left[\frac{1.99\text{mm}}{102\text{mm}}\right] = 1.1 \text{ degrees.}$$

Similarly, the detector has a viewing angle $\emptyset_D$ whose tangent is similarly defined and with a detector portal five millimeters in diameter and 150 millimeters long. The value of $\emptyset_D$ can therefore be calculated as

$$\emptyset_D = \tan^{-1}\left[\frac{D}{L}\right] = \left[\frac{0.5\text{cm}}{15\text{cm}}\right] = 1.9 \text{ degrees.}$$

The maximum angle within which the detector can accept scatter is the sum total of these angles, which equals three degrees. It must now be shown that the scattered radiation detected is small compared to the primary signal for a cobalt-60 beam with these collimation restrictions.

If N_0 is the photon flux which would enter the detector if no scattering medium were present, x the distance traversed within the medium before scatter takes place, σ_e the scatter coefficient for the angle of acceptable scatter derived from the Klein-Nishina formula, dNe the scattering medium, and D-x the distance within the medium which

must be traversed after the scattering event, then the number of scat-
tered photons reaching the detector per steradian will be

$$dNs = No \cdot \exp(-\mu_{abs} \cdot x) \cdot \sigma_e \cdot dNe \cdot \exp(\mu_{att} \cdot (D-X)) \qquad 4.2$$

Combining terms

$$dNs = No \cdot \sigma_e \cdot dNe \cdot \exp(-x \cdot (\mu_{abs} - \mu_{att}) - \mu_{att} D) \qquad 4.3$$

Since some photons will be scattered but not absorbed in the distance
x, these photons will be available for further scatter. The absorption
coefficient is therefore used for the x interval. Once a photon is
scattered into the detector's angle of acceptance, any further inter-
action will likely remove it from the path of acceptance. Therefore,
the term used to describe the second region of interaction, D-x, util-
ized the linear attenuation coefficient. To simplify Equation 4.3 it
will be assumed that all of the scatter for an entire thickness D will
occur in a one centimeter strip in the center of the volume. As in
the previous assumptions, this yields a worse than actual case situ-
ation. Equation 4.3 can now be reduced to

$$dNs = No \cdot \sigma_e \cdot dNe \cdot \exp(\mu_{att} \cdot (.5-D) - .5\mu_{abs}) \qquad 4.4$$

In view of the assumptions the integration of dNs is simply Ns, the
total number of scattered photons, and dNe is the sum of electrons in
the scattering thickness D. This further reduced Equation 4.4 to

$$N_s = N_o \cdot \sigma_e \cdot \sum N_e \cdot \exp(\mu_{att}(.5-D)-.5\mu_{abs}) \qquad 4.5$$

If it is assumed that all of the scatter is through the angle with the largest scatter coefficient, σ_e will be 7.9×10^{-26} centimeters^2 per electron per unit solid angle. Since the radiation will be isotropically scattered into a unit solid angle, the number of scattered photons N_s must be multiplied by the fraction of a steradian which the detector occupies. The detector with a diameter of 0.5 centimeters will always be at least 20 centimeters from the scattering medium. The portion of a steradian it occupies is

$$\text{angle} = \frac{6.5}{4} \cdot \frac{1}{(20)^2} = 0.001 \text{ steradian}.$$

Table 4.1 was obtained from Equation 4.5 for tissue thicknesses ranging from one centimeter to 40 centimeters. Column II of Table 4.1 was obtained by dividing both sides of Equation 4.5 by N_o, the total photon flux, while column III was obtained by dividing Equation 4.5 by the number of photons, N_{tot}, reaching the detector, where

$$N_{tot} = N_o \exp(-\mu_{att}D) \qquad 4.6$$

It can be seen that the maximum scatter fraction of the total beam is 4% per steradian for 40 centimeters of tissue.

Examining Columns II and III of Table 4.1, it can be seen that the amount of scatter radiation reaching the detector, for varying patient thicknesses, reaches a maximum at a depth of 20 centimeters after which it decreases. This is what would be expected since the maximum penetrating distance of the scattered radiation for cobalt-60 is 20 centi-

TABLE 4.1

TISSUE THICKNESS VERSUS SCATTERED RADIATION

Tissue Thickness	Percent of initial photon beam scattered into the detector per unit solid angle	Percent scattered radiation of total detected beam per unit solid angle
1	.025314	.027
2	.047963	.057
3	.068747	.0387
4	.087399	.1215
10	.162541	.373
15	.187854	.663
20	.197180	1.0498
30	.175864	2.21
40	.148940	4.14

meters. On the other hand the ratio of scattered radiation to the amount of total beam penetrating the patient continually increases with increasing thickness.

Collimation Shield

The use of an isotope in place of an x-ray tube requires that the source be shielded whether the beam is effectively "on" or "off." The shield must also have the ability to automatically return the isotope to the "off" position in the event of a loss of system power.

With these requirements in mind, it was decided to combine the shield and primary collimation into one solid unit. The source, a one millimeter by one millimeter by two millimeter cobalt-60 pellet, is encapsulated onto a rod and is held in the center of a shield when in its "off" position. To produce the transmission beam, the rod is drawn back, bo a solenoid, approximately one centimeter, so that the source is aligned with a straight bore collimator. In moving the rod to this extracted position a spring which will return the source to the "off" position is compressed whenever the solenoid is deenergized. This design, having only one moving part, maximizes reliability and safety.

The next step in the design was the selection of a material from which to build the shield collimator. Irregardless of the material chosen, the amount of attenuation required from the shield must be the same. If x is the fractional decrease in beam intensity required, it is defined as

$$x = \exp(-u_{\ell}r)$$

Where μ_ℓ, is the linear attenuation coefficient of the shielding material being used and r is the linear thickness of attenuating material. Solving for the linear thickness of attenuating material

$$r = \frac{\ln(1/x)}{\mu_\ell} \, .$$

This defines the length of material which must be traversed as a function of beam reduction and linear attenuation coefficient. If a spherical shield-collimator is to be built, the volume required would be

$$volume = \frac{4}{3}\pi r^3 \, ;$$

substituting the attenuating thickness for the radius

$$volume = \frac{4}{3}\pi (\ln(1/x))^3 (1/\mu_\ell)^3 ;$$

if then all constants are combined and set equal to C_1

$$volume = C_1 (1/\mu_\ell)^3 .$$

The weight of this sphere would simply be the volume times the material density

$$weight = C_1 (1/\mu_\ell)^3 (\rho)$$

where ρ is the density of the material.

$$\mu_\ell = (\mu_m)(\rho)$$

here m is the mass attenuation coefficient. The weight can be expressed as a function of μ_m and ρ:

$$\text{weight} = C_1 (1/\rho)^2 (1/\mu_m)^3.$$

Dropping the constant C_1 and evaluating this expression for lead, tungsten, and depleted uranium, it can be seen in table 4.2 that the weight can be minimized through the use of depleted uranium.

There exists, however, a problem with the machining of special atomic materials such as depleted uranium and a compromise had to be made between the shield shape, weight, and ability to securely mount it on the scanner. Because of the problems associated with sliding depleted uranium against itself, the source was encapsulated onto a tungsten rod. The final collimator shield and the two-section couch can be seen in Figure 4.4. The resultant design utilizing depleted uranium weighed approximately 260 lb., which is in contrast to the 600 lbs. of lead which would have been required for the equivalent shielding.

TABLE 4.2

EVALUATION OF SHIELDING MATERIALS*

	Density	Mass attenuation coefficient	Relative weight
Lead	11.35	0.698	22.83
Tungsten	18.00	.05755	16.19
Depleted Uranium	18.35	.0669	9.92

* these numbers reflect only primary attenuation and do not reflect the effect of build-up factors.
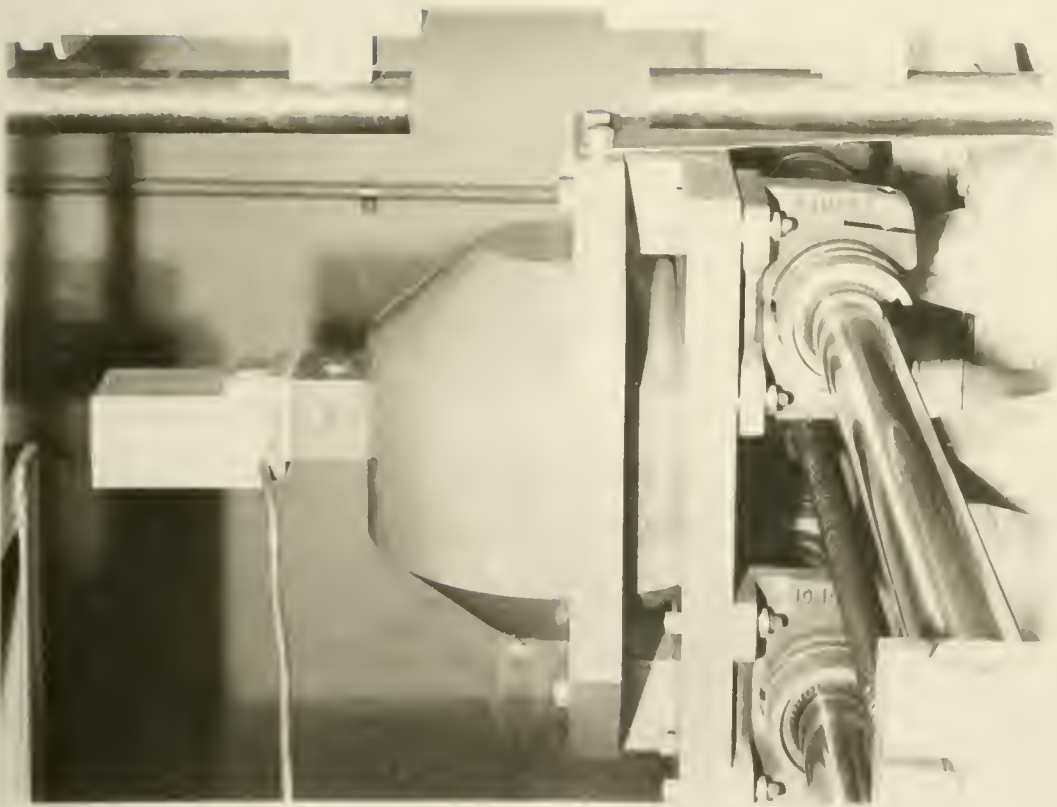
Figure 4.4.   Collimator Shield and Couch.

CHAPTER 5

ELECTRONIC LOGIC DESIGN

Overview

At the beginning of a scan the detector and source, as well as the
rotational system, must be positioned. This is conveniently achieved
through the use of specially positioned microswitches. The source and
detector are brought up to a constant speed of 4 centimeters per second
by a digital ramping sequence over a 6.6 millimeter distance. Once
full speed is achieved, the measuring of transmission data begins.
These transmission measurements continue until the source and detector
are 6.6 millimeters from the end of the traverse. At this point, the
transversing system is ramped down to a stop. The rotational drive motor
is then pulsed and a rotational shift is begun. After rotation has been
completed, the second traverse is initiated and proceeds identically to
the first but in the opposite direction. This process, of alternating
traverse scans and rotations, continues until the scanner is in an
orientation 180° from its original position.

A digital computer was designed and fabricated to control the
traverse and rotational sequences and the data aquisition system.
Complimentary Metal Oxide semiconductor circuitry, CMOS 4000 series
was used. This circuitry was primarily selected for its low power con-
sumption and its noise immunity. Since speed was not a concern, it

46

proved adequate for all switching requirements. The controlling elec-
tronics can be subdivided into five categories; the clock, the sequence
controlling logic, the ramping logic, the data acquisition logic, and
the motor driving logic.

The sequence control logic initiates each traverse and at the tra-
verse completion, initiates and terminates the required rotational shift.
This circuitry also terminates the scanning sequence and resets the ap-
paratus to its reset orientation. The ramping logic, upon a signal from
the controlling logic, fabricates a positive accelerating eight step
ramp at the initiation of each traverse. The data acquisition system
controls the electrometer amplifier and provides the signals to properly
sequence the recording system. The motor driving logic provides the
various motors with the proper sequence of pulses for either clockwise or
counter-clockwise operation.

The Clock

The entire scanning procedure is dependent upon the signals from the
system clock. The choice of a 4047, used as an astable multivibrator, was
made based upon its stability, less than 0.5% deviation at 40 kilohertz,
and the availability of easily adjusting its output for experimentation.

During initial setup, the clock pulses were observed on the ten volt
supply. Although it seemed unlikely that the 4047 was the cause of the
problem, it was decided to isolate it from the power supply as shown in
Figure 5.1 (the 4050 gates shown in the figure are actually six gates
tied together). A switch which makes available the 4047's oscillator
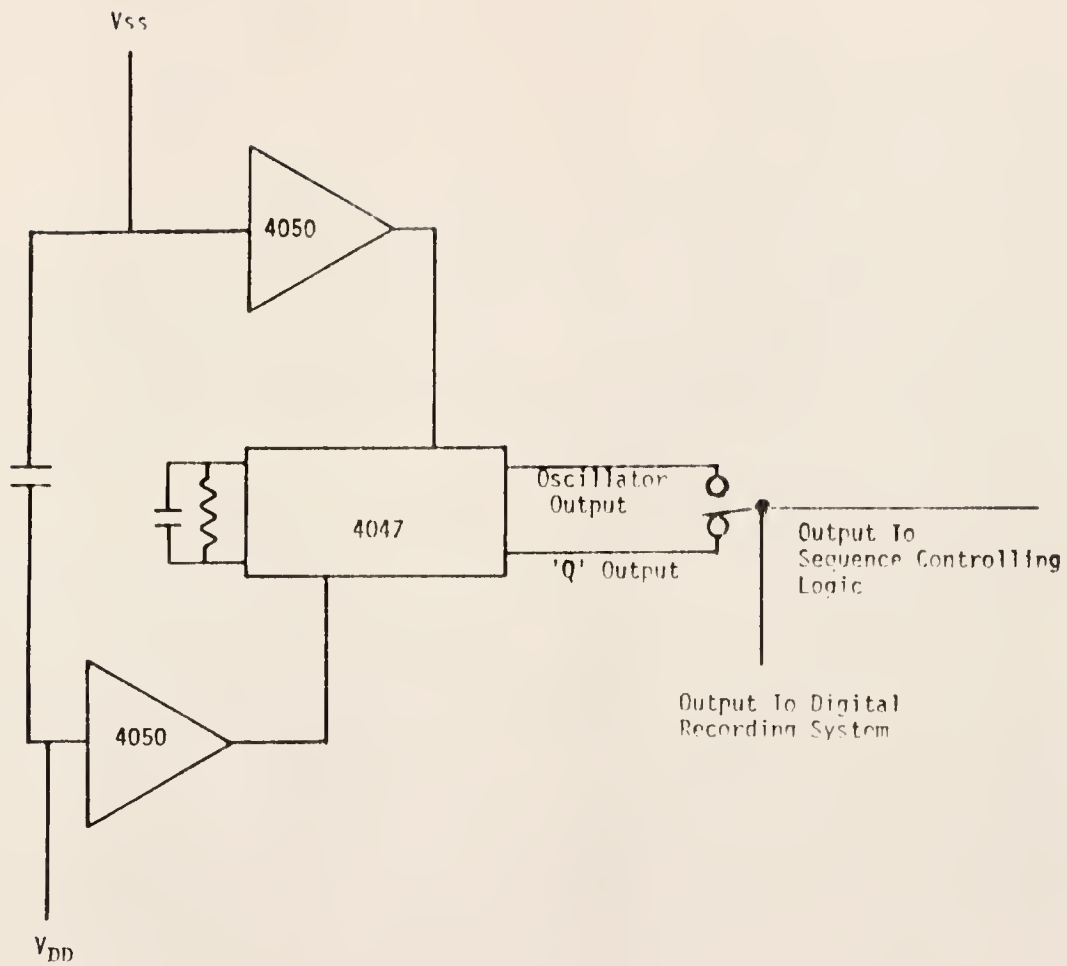output was installed to enable faster manual positioning of the drive
system.

Figure 5.1. Diagram of the clock circuit.

The Sequence Controlling Logic

The main logic control was fashioned after a similar design used by Fitzgerald (1974). It allows the alternating of traverse and rotational movements and a means for resetting the scanning apparatus. The logic Figure 5.2 shows the basic system design.

The pulses originate at the main clock, AB, and are divided by a seven-stage binary counter, AA. This arrangement is used to provide the nominal 24 kilohertz signal required by the ramping, r, and r circuits and also makes available a 50 kilohertz signal required by the digital recording system. When the equipment originally is switched on, the SCR conducts and gate V sends a reset pulse to all counters, including the ramping electronics. In this reset condition, the ramping electronics divides the incoming pulse by 100.

The clock pulses do not progress further than NAND gate S, which has one input held low by the anode of the SCR. Pulses are, however, supplied to relays R1 through R4 which allow manual control of the various motors for initial position. When any one of the four manual relays are switched from their scan mode to a manual mode, the gate W sends the SCR into conduction and therefore all counters are sent into reset. This arrangement is used so that once manual control of the unit is assumed, a deliberate effort must be made to restart the scanning procedure.

The initiation of a scan involves the setting of the start switch S1 to low. This inhibits the bilateral switch X from conducting, thus causing the current through the SCR to drop therefore stopping its conduction. Once the SCR ceases to conduct, its anode goes high and
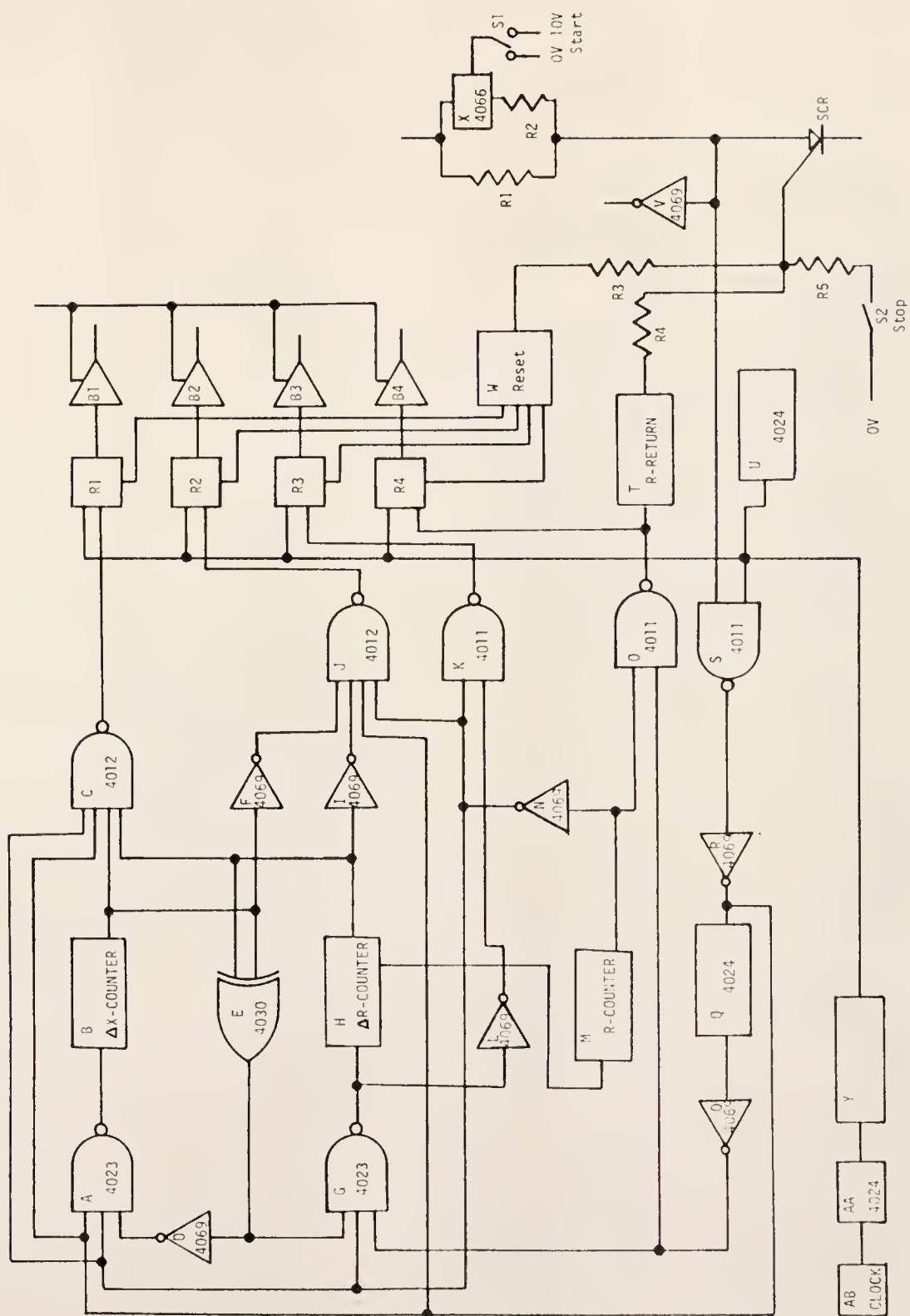
50

Figure 5.2. Diagram of Sequence Controlling Logic.

the output of gate V goes low taking all appropriate counters out of reset. Simultaneously, the inhibiting output of gate S is brought high allowing clock pulses to be transmitted and the scanning procedure to be initiated. The pulses being passed by gate S are inverted by inverter R which delays them one half pulse, and then go to the transverse and rotational sections. The ramping logic Y is arranged so that it is in reset when a rotation is made. Therefore, the pulses from counter AA are being divided by 100, resulting in a 2.4 kilohertz signal available for control of rotational motors which requires a 40 hertz pulse train. In order to reduce the frequency of this pulse train, counter/divider Q is used. Since this counter also inverts the signal, inverter D is used to resynchronize the pulse train.

Throughout the entire scanning sequence, pulses for translation and rotation are being sent to gates A and G, which run to the Δx and Δr counters respectively, and to gates C and J. Since all counter outputs are low after a reset pulse, the Exclusive-OR gate E has a low output, prohibiting passage of rotational pulses through gate G. The low output of the r counter also inhibits gate O from passing pulses to the rotational drive system. When the three inputs to NAND gate J are high, the pulses for translation are passed to relay R2 and the driver buffer B2. The function of the buffers B1 through B4 is to provide enough current to drive the TTL loads of the motor drivers and also to drop the voltage of the logical high from positive ten volts to positive five volts.

Once the x counter has received a preset number of pulses, the number being dependent upon which scan width has been set, its output goes high. This results in gate E going high, gate A ceasing to conduct pulses, and gate G permitting the conduction of pulses for a

rotation. The pulses for rotation are passed through inverter L to gate K, and to relay R3 and buffer B3 which enables a counter-clockwise rotation. Once the predetermined number of motor pulses have been accumulated, the Δr counter goes high, sending gate E low which inhibits pulse conduction through gate G and enables the conduction through gate A. The level changes of the Δr counter also places an inhibit on gate J and removes the inhibit from gate C. This sends the motor driving pulses through relay R1 and buffer B1 which drive the translational system in the direction opposite to the previous traverse. Once this translation is completed, the Δx counter goes low sending gate E high. The termination of this translation once again initiates a rotation. The rotation, again, sends pulses through gate K and once the preset number of rotational counts have been reached, the next traverse is begun.

After every other traverse, the Δr and Δx counters are in their initial state; therefore, the only change in the circuit is the accumulation of pulses being sent to the rotational system by the r counter. When the scanner has reached an orientation 180° from its initial traverse, the r counter goes high. This switches inverter N output to a low inhibiting conduction through gates A, C, G, and K while enabling pulses to pass through gate O. The rotational drive signals pass through gate O and to relay R4 and the r return counter, T. The sending of pulses through relay R4 causes rotation in a clockwise direction until counter T goes high. The signal from the counter places a ten volt high, via a 10^4 ohm resistor, on the gate of the SCR causing it to conduct. This sends the base of the SCR low, the output of counter V high, and all counters into reset. The circuitry stays in reset until another scan is initiated.

Ramping Logic

Transverse Motion

In order to achieve a transverse speed of four centimeters per
second, the stepping motors must operate at a pulsed rate of 720 pulses
per second or one pulse every 1.38 milliseconds. It was determined
through experimentation that the motors would not respond, under load, to
an initial pulse rate in excess of 120 pulses per second or one pulse
every 8.3 milliseconds. In order to accelerate the motors to and from
the required speed a digital ramping sequence was employed. The logic
for this sequence can be broken into two sections. The first section,
Figure 5.3 determines when in the traverse a ramping sequence is to be
employed and when a constant traverse speed is to be maintained. The
second circuit, Figure 5.4 actually takes the incoming clock pulses and
produces a pulse sequence, either increasing in period or decreasing in
period, depending upon whether a negative or positive acceleration is
required.

The initiation of the acceleration is controlled by gate G of
Figure 5.3 while the sign of the acceleration is determined by NAND
gate C of Figure 5.5. The frequency reduction is achieved through the
use of counter T of Figure 5.4, a programmable divide-by-"N" counter,
4059. This integrated circuit has the ability to divide an input pulse
train by any integer between three and 15,999 inclusive. The output signal
is a positive pulse one clock pulse wide occurring at a rate equal
to the input frequency divided by N, the divide-by number. The divide-
by number is programmed into the counter through a 16 jam input. By
altering these inputs, the output is accordingly altered. Table 5.1
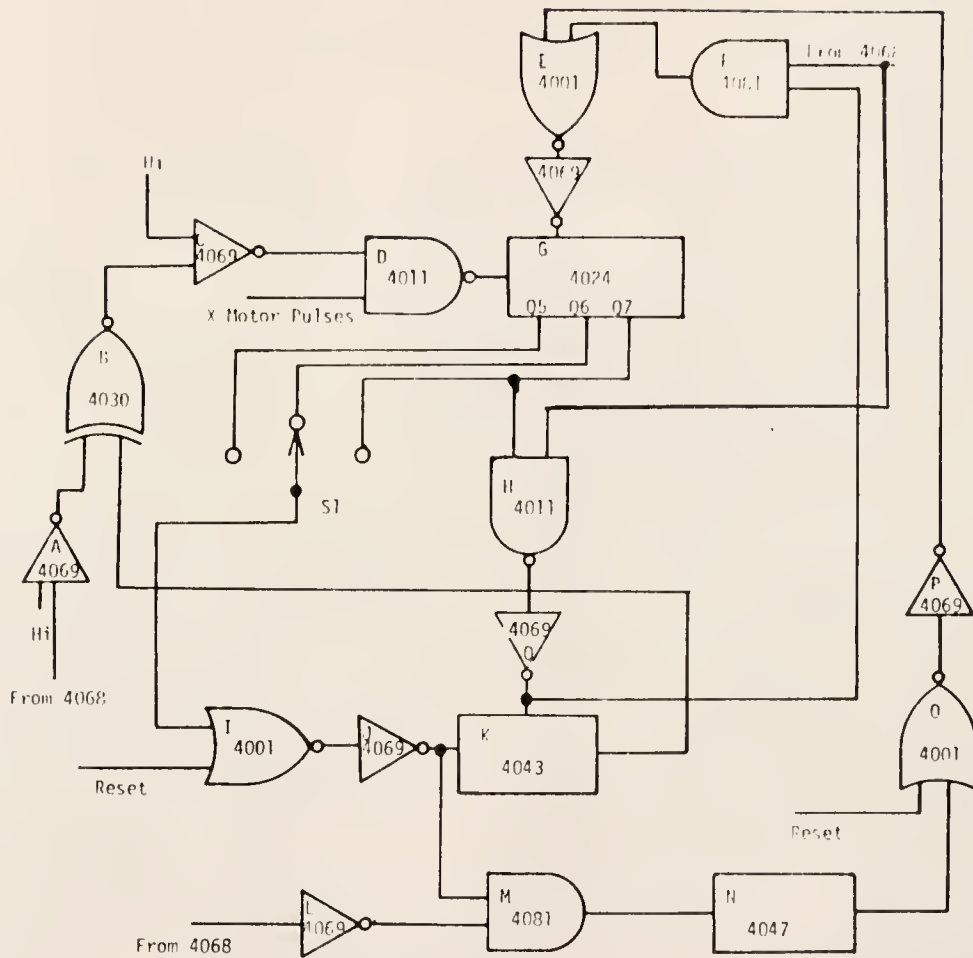shows the pulse rate for the various ramping steps and their frequency.

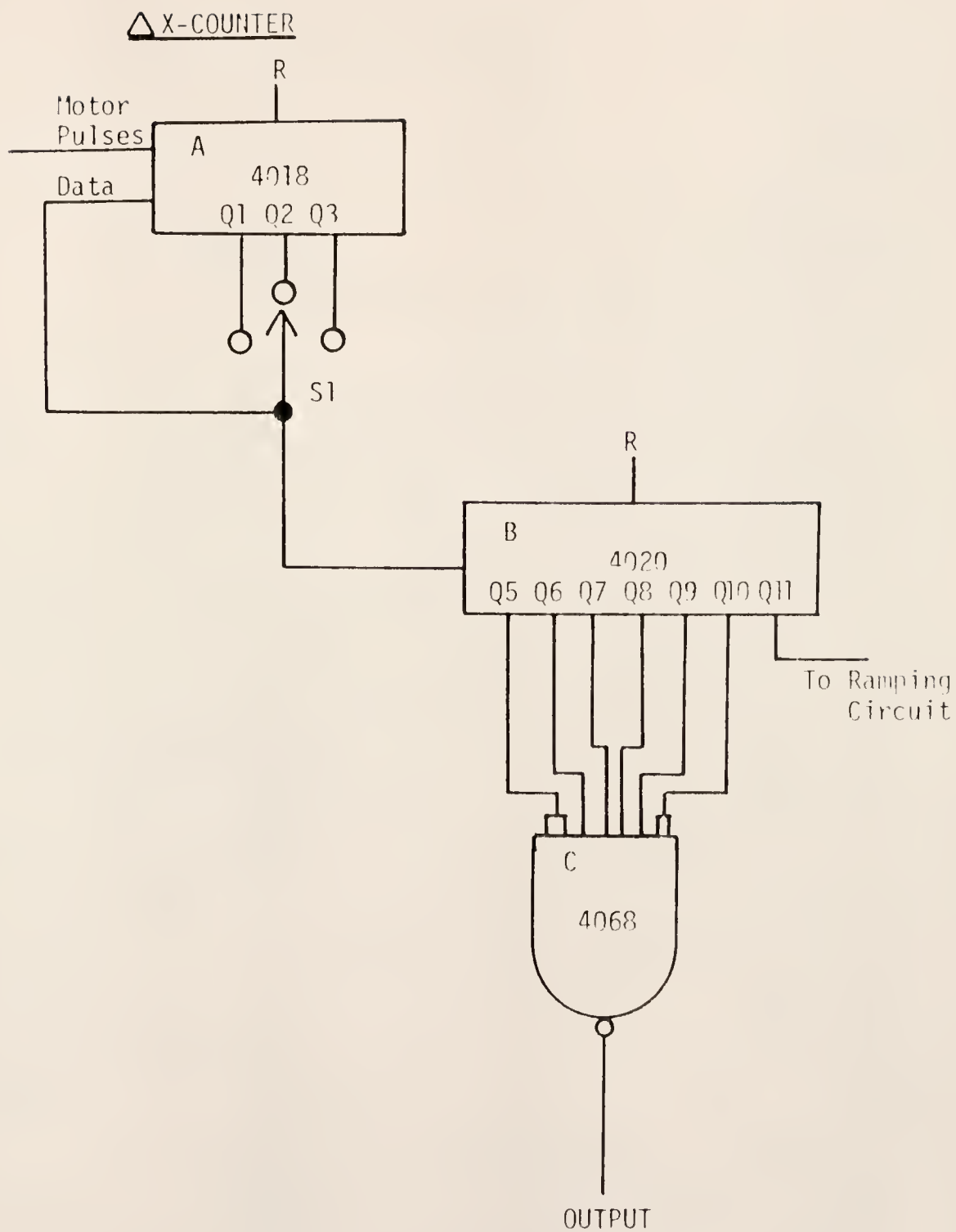Figure 5.3. Diagram of the Ramping Controlling Logic.

Figure 5.4. Diagram of the Ramping Counter-Divider Circuit.

Figure 5.5.   Diagram of the ΔX Counter.

TABLE 5.1

RAMP INTERVAL SPECIFICATIONS

Ramp Interval	Time between pulses (milliseconds)	Percent of full speed	Change in speed as compared to previous step	Divide by integer #
1	8.31	32		100
2	6.32	42	29%	76
3	4.25	63	49%	50
4	3.82	70	11%	46
5	3.32	80	15%	40
6	3.16	84	5%	38
7	2.99	88	6%	36
8	2.83	94	6%	34
9	2.66	100	6%	32

As can be seen by the fourth column of Table 5.1, there exists
no obvious pattern to the ramp sequence. It was determined by experi-
mentation and the only comment that can be made is that it works properly.
The unusual step pattern dictates that the final integer used as the
divide-by number not be the lowest integer possible, i.e. three.
This is simply because the next higher divide-by integer, four, would
dictate the last step in the ramp to be an increase in speed of 33%.
It was therefore determined that during the full-speed traverse the
pulses would be the result of a divide-by-32, allowing the selection
of the previous step to be a divide-by-34, an increase in speed of only
6%.

The selection of the programmed divide-by integer is accomplished
through the use of a set of AND gates, actually one NAND gate is employed
but its output is inverted to make it equivalent to an AND gate. The
input of the AND gate is one of a pair of Decade Counter/Dividers, counters
K and L of Figure 5.4.

Since it is desirable to use the same set of gates for the positive
as well as negative accelerating ramps, an up-down decade counter is re-
quired. At the time this circuit was designed, this specific piece of
logic was not available as a single integrated circuit so the equivalent
of an up-down counter was fabricated. It uses two 4017 Decade Counters
and 16 bilateral switches, which tie the output of the two counters
together,(see Figure 5.4). This circuit is arranged such that during the
positive accelerating ramp the input to inverter D is high, thus putting
the 4066s whose inputs are tied to counter K in a conducting mode and
allowing the outputs of that counter to control the jam input of the
4059. The 4066s tied to counter L have their outputs floating, thus
effectively taking counter L out of the circuit. During the negative

acceleration, at which time the input of gate D is low, counter K controls the jam inputs of the 4059 while counter L is isolated. This circuit also holds the decade counter not being used in reset so it does not accumulate pulses during the opposite ramp.

The two counters K and L of Figure 5.4 are arranged so that the "eight" output of counter K is exchanged, during the transition from negative to positive ramping, with the "0" output of counter L, while the "seven" output of counter K is exchanged with the "one" output of counter L, and so on. Since counter L is in reset when counter K has reached its "eight" output, the transition from positive to negative does not occur until counter L accepts its first pulse and its "one" output goes high.

The pulses which control the ramping sequence are identical to the pulses which trigger the motor controllers. Since it was necessary to have each ramp step exist for more than one pulse the pulses are divided by counter H, Figure 5.4, which is set for a divide-by-eight mode. Since eight ramping steps are required the entire sequence takes 64 motor pulses, however, full speed is not achieved until the 65th motor pulse has been received. This is due to the internal design of the 4059, counter T, which only transfers the jam input to buffers after each output pulse. Since the divide-by-32 is programmed after the 64th pulse the counter must go through one more cycle of the previous divide-by mode, i.e. 34, before the transfer of the jam input occurs.

Ramping Sequence

Since the beginning of the first traverse, latch K of Figure 5.3 has been left in a reset state; gate C of Figure 5.4 is allowed to pass pulses to counter H. The reset pulse has also left gate C of Figure 5.5 the ramp sign pulse, high. This sets both inputs of exclusive

OR gate B of Figure 5.3 low, allowing clock pulses to pass through gate D to counter G. For the remainder of this discussion, it will be assumed that the logic is set for a scan width of 31 centimeters, i.e. a divide-by-six mode for Figure 5.3, Figure 5.4, and Figure 5.5.

As counter G of Figure 5.3 accumulates pulses, its output Q_6 goes high placing a reset pulse on latch K. Since this latch has been left in reset, the pulse has no effect on the circuit. As Q_7 of counter G goes high, NAND gate H goes low and latch K changes levels to a low. This level change puts a low on the input of gate C of Figure 5.5 inhibiting pulses to counters K and L. At this time, 64 motor pulses have passed and counter K of Figure 5.4 has its output "eight", pin nine, high setting the jam input of counter T for a divide-by-32, i.e. for full speed ramping. This pulse also puts a low on one of the inputs of gate B of Figure 5.3 inhibiting pulses to counter G.

This state exists until counter B of Figure 5.5 reaches a count of 1008 (depending if the divide-by-four, divide-by-six, or divide-by-eight mode has been selected, this will be 128, 192, or 256 pulses respectively from the end of the traverse). This allows NAND gate C of Figure 5.5 to go low which in turn allows gate B of Figure 5.3 to go low and permitting clock pulses to pass to counter G. When inverter Q of Figure 5.3 went high to set latch K it also reset counter G. Counter G now accumulates pulses until it reaches a count of 32 and Q_6 goes high. This resets latch K to a high. Since the pulses were allowed to pass to counter G when 192 pulses were left in the traverse, there exists 128 pulses till the end of the traverse. If the 21 centimeter scan width was in use, the switches of Figure 5.3 and 5.5 would be set for the divide-by-four mode. This would mean that when gate A goes low only four times 16 or 64 pulses are left in the ramp and allow the first pulse which passes

through counter G of Figure 5.3 to initiate the negative ramping sequence. Likewise, if a 40 centimeter ramp were used, i.e. the divide-by-eight mode, eight times 16 or 128 pulses would be left in the ramp and latch K would not change state until 128 pulses had passed.

Upon completion of the last 128 motor pulses of the traverse, counter T of Figure 5.4 is brought to the divide-by-100 mode in eight steps identical to those which were used for the positive acceleration. Upon completion of the traverse, gate C of Figure 5.5 would once again go high and the next pulses sent to the traversing motors would initiate the next ramping sequence.

ΔX Circuit

The traverse is controlled by the Δx circuit. The circuit con- sists of a presetable divide-by-"N" counter, CMOS 4018, a 14 stage ripple-carry binary counter/divider, CMOS 4020, and an eight input NAND gate, CMOS 4068, (see Figure 5.5). The clock pulses received by counter A are identical to those sent to the motor driver boards. Switch S1 allows the incoming pulses to be divided by either four, six, or eight nominally for the 20, 30, or 40 centimeter scan widths respectively. The pulses required to traverse the various widths are 4096 for 20 centimeters, 6144 for 30 centimeters, and 8192 for 40 centimeters. The choosing of higher divide-by numbers results in more total clock pulses being re- quired to send the Q_{11} output of the 4020 high. Depending upon which scan width is desired, the output of the Q_{11} will go high after the appropriate number of pulses have been accumulated, thus signifying the end of a traverse and the initiation of a rotational shift.

The purpose of the NAND gate C is to signify, by going low, that the 4020 is 32 counts from the end of the traverse. This signal is used

by the ramping circuit to initiate a countdown procedure which will first inhibit the electrometer amplifier circuit and secondly ramp the traversing motion to a stop.

∆R Circuit

Unlike the ∆x circuit, the number of pulses required for completion of rotational shifts was not a convenient power of two. It was found that a total of 6228 pulses were required for 180° of rotation. In order to have 36 views, one view every five degrees, 173 motor pulses are required per rotational shift. For other rotational shifts, i.e. ten degrees, 346 pulses are required and 20 degrees, 692 pulses are required. The pulse signifying the termination of rotation was achieved by the use of the circuit in Figure 5.6 the ∆r circuit.

The clock pulses going to counters A and B are identical to those being sent to the rotational stepping motor controller. These counters are wired into an eight input NAND gate, one gate in such a manner as to trigger a low on the accumulation of 173 pulses. NAND gate C going low increments counter D by one and resets counters A and B enabling the next count of 173 to again send gate C low. A specific output of counter D can be selected through the use of switch S1. The ∆r counter output will then go high on either 173, 346, or 692 pulses which correspond to 5, 10, and 20 degree rotational shifts.

R Counter

The r circuit, Figure 5.7, receives its input from the r circuit, Figure 5.6. As gate C in the ∆r circuit counts to 173 and sends a pulse to counter D, the A counter of the r circuit receives the same pulse. When the circuit has accumulated 36 pulses, the output of inverter C
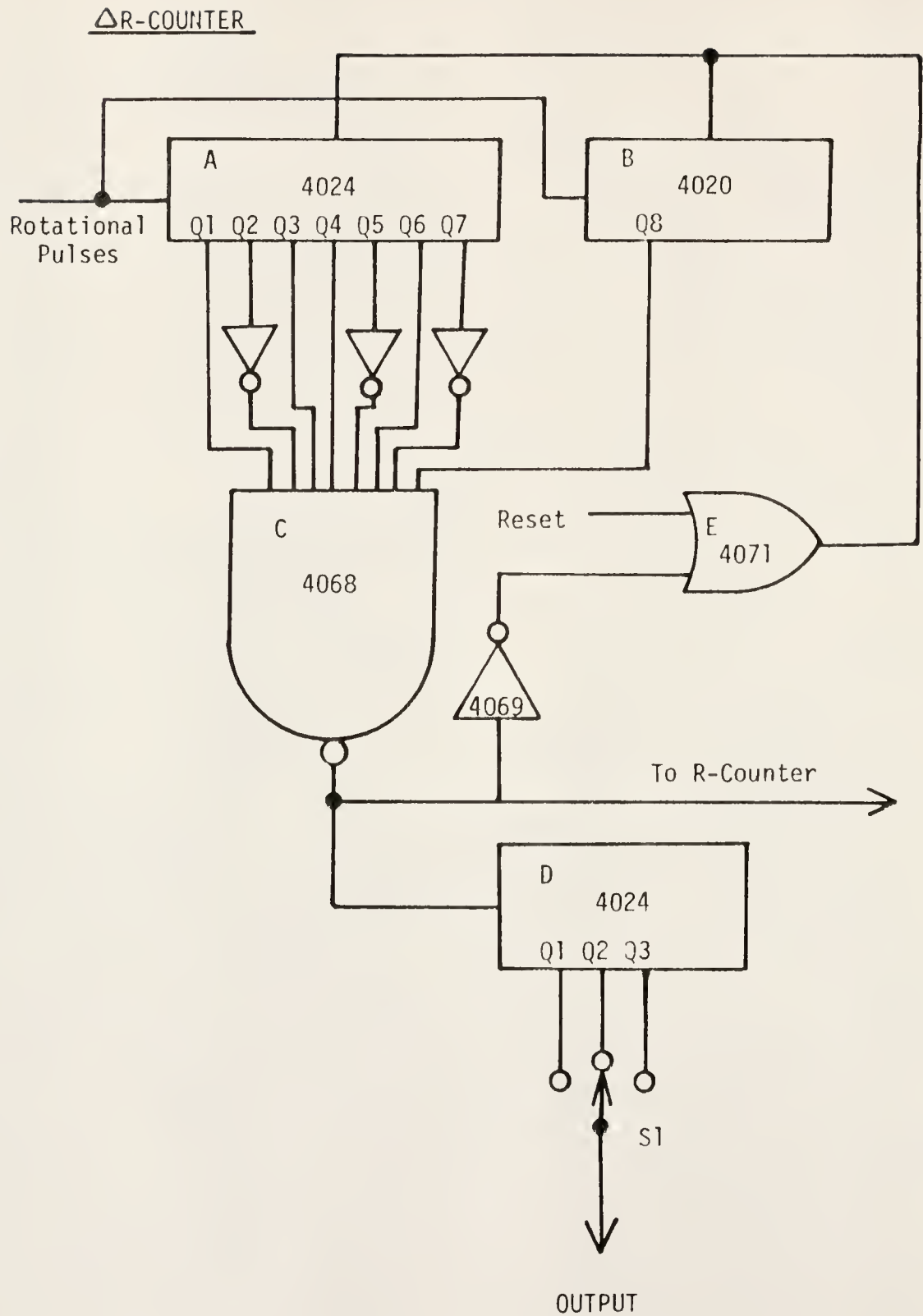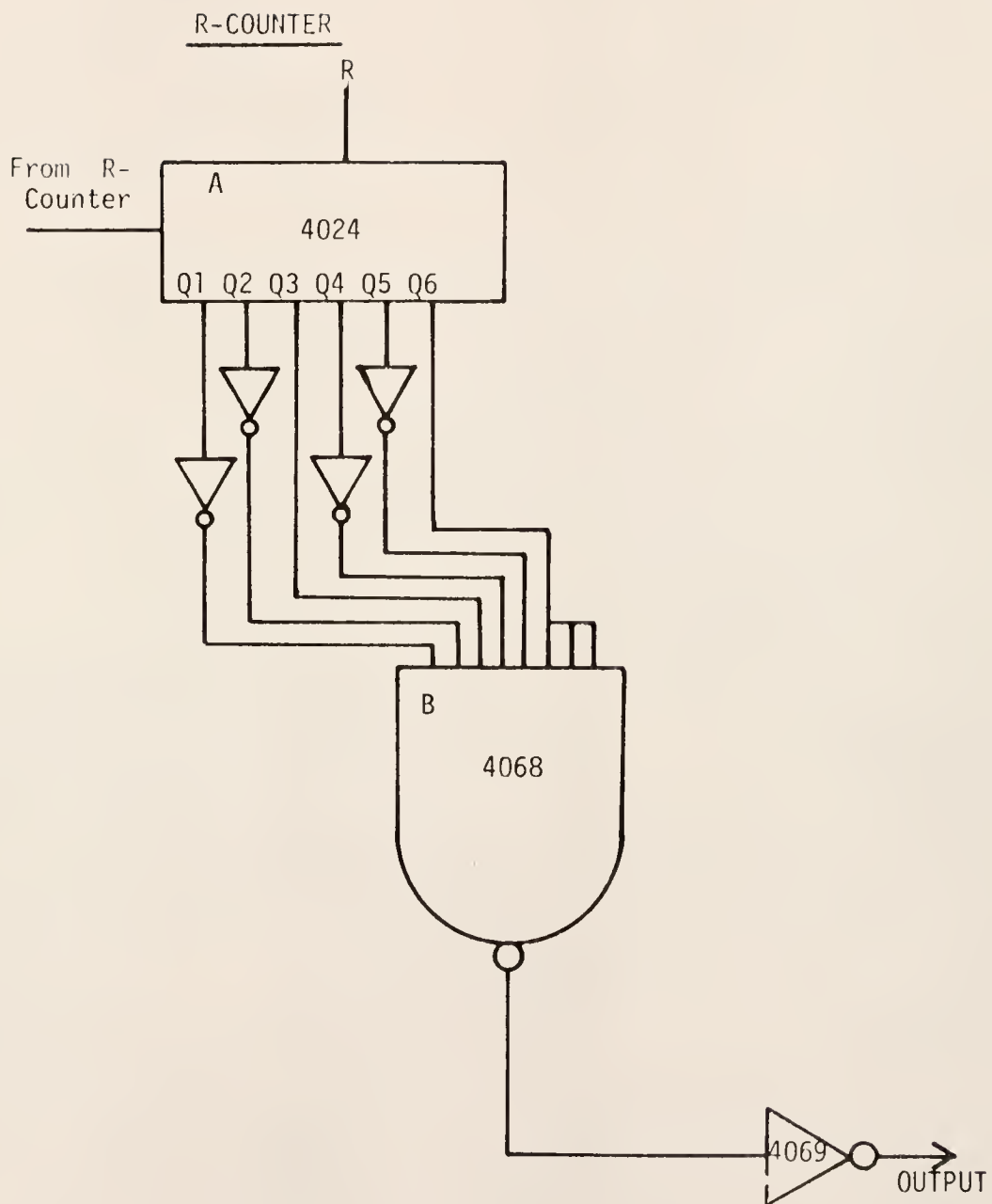
Figure 5.6.   Diagram of the ΔR Counter Circuit.

Figure 5.7.   Diagram of the R Counter Circuit.

goes high. This signifies the end of a scan and the initiation of the reset procedure.

Motor Controlling Logic

In order to properly sequence a stepping motor, either clockwise or counter-clockwise, the various windings must be energized in a sequence particular to each motor and set by the motor's physical design. Each stepping motor manufacturer makes available control circuitry tailored to their specific motor's requirements. It was decided to utilize such circuitry for all stepping motors used on the cobalt-60 scanner.

The control boards for the Warner motors provide pulses to two sets of windings simultaneously in an attempt to obtain more torque. Each of these pulses is composed of two voltage levels. At the beginning of the pulse a 50 volt pulse is initially applied to the motor to obtain high starting torque. The motors, however, can not dissipate enough heat if 50 volts were used for the entire pulse. Therefore, at the preset time, the controller switches from the 50 volt pulse to a 12 volt pulse.

The input requirement for the controller is a negative going five volt pulse not shorter than ten microseconds duration.

The Slo-Syn motor used for rotation performed adequately with a single voltage pulse. The manufactured motor controller was used to correctly sequence the energizing of the windings for clockwise or counter clockwise operation.

CHAPTER 6

DATA ACQUISITION

In order to obtain the data required for reconstruction, $P(ma,\emptyset)$ of Eq. 3.24, the current signal being produced by the photomultiplier tube must be recorded. It was decided to use a method of repetitive integrals, Fitzgerald (1974), to obtain these measurements. This has been proven to be an effective method to measure small currents without experiencing a shift of the data, due to a resistor-capacitor time constant.

In short, this method uses an integrating amplifier with a long time constant, i.e. typically 100 seconds. The voltage output of the amplifier is sampled near the beginning of the integrating cycle and again near the end. The difference in these readings is assumed to be the accumulated current value for that interval. The amplifier is then reset and is ready for the next integrating cycle. The average signal over the interval is taken as the instantaneous current at the center of that interval. The smaller the sampling intervals become, the closer the mean current is to the actual current. Theoretically, if the measuring intervals were infinitely small the measured transmission profile would equal the true profile. However, it has been shown (Fitzgerald, 1974), that intervals of 3.3 millimeters would be sufficient.

Electrometer Amplifier

In its original application, the repetitive integral method was used to measure currents as low as a few picoamperes. The signal available from the photomultiplier tube (for the cobalt-60 scanning application) is orders of magnitude above that level. The photomultiplier tube voltage versus current curve can be seen in table 6.1. These larger currents enabled the circuit, used by Fitzgerald, to be simplified to that of Figure 6.1. One problem was encountered however, due to these higher currents and that was being able to reset the amplifier within the restraints of the amplifier cycle time.

The resetting of the circuit is achieved by discharging capacitator C1. Since the currents involved in Cobalt-60 scanning are much larger than those of Fitzgerald's original application, the capacitor 's size and the charge which must be dealt with during reset are also larger. The transistor used to reset the capacitor must also have a high enough off resistance to impede leakage currents, which would in turn cause amplifier nonlinearity. Of the transistors available at the time of fabrication, none met these dual specifications.

One solution was found in the use of series bilateral switches, CMOS 4066. This switch has low on-resistance, typically 80 ohms, and low off-leakage current, less than ten picoamperes at ten volts.

The problem of leakage effecting the amplifiers linearity was examined by placing a constant current source on the input of the amplifier and recording output voltage versus time. The response of the amplifier, using four bilateral switches tied in series and an integrating capacitor of 80 nanofarads, is shown in Figure 6.2. As can be seen, the response was linear over a 250 second integration interval.

TABLE 6.1

CURRENT VERSES VOLTAGE FOR THE
NaI(Tl) DETECTOR SYSTEM

Tube Voltage (Negative High Voltage) volts	Tube Current (Source on) 10^8 amps
100	0.0011
200	0.0021
300	0.0035
400	0.0084
500	0.0289
600	0.1040
700	0.3280
800	0.9050
900	2.240
1000	4.390
1100	9.080
1200	17.65
1300	32.30
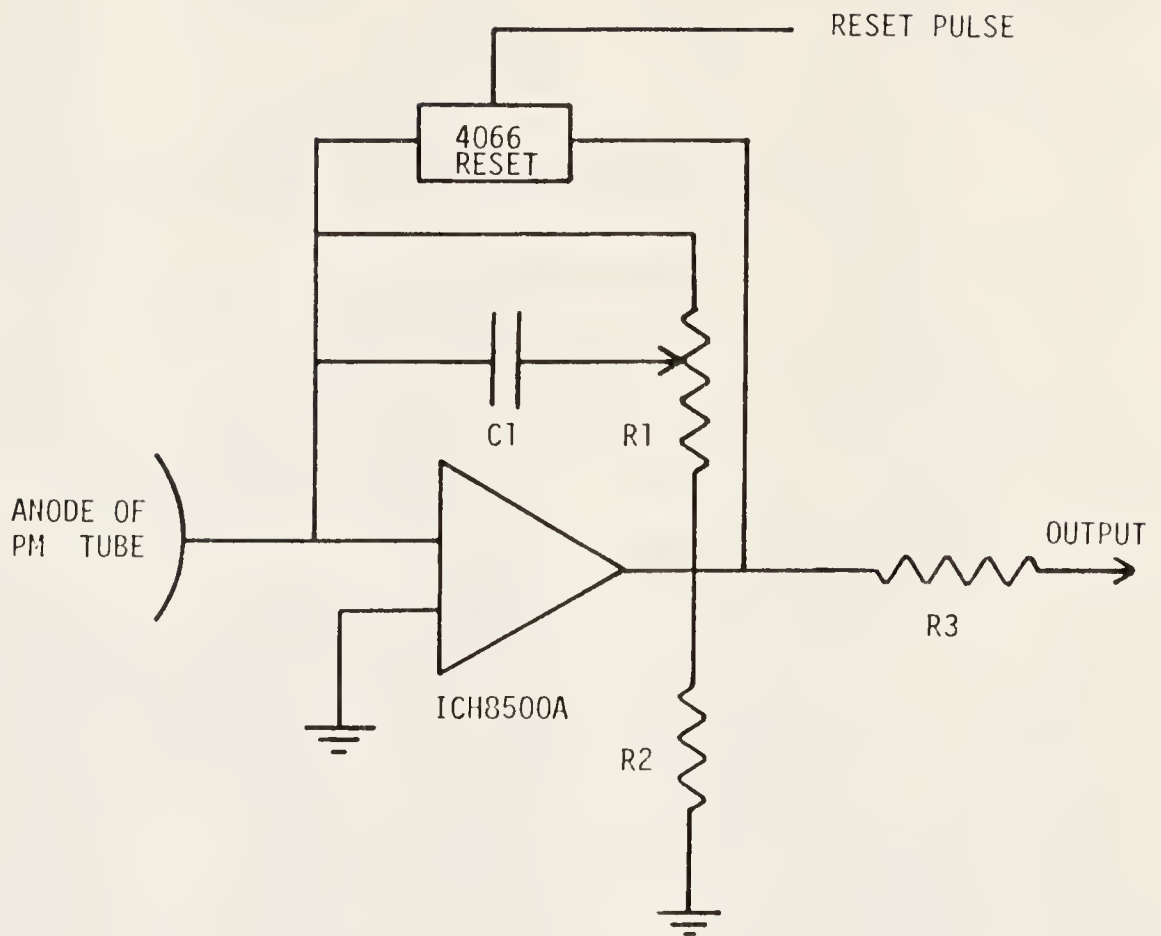
Figure 6.1.   Diagram of the Electrometer Amplifier Circuit.
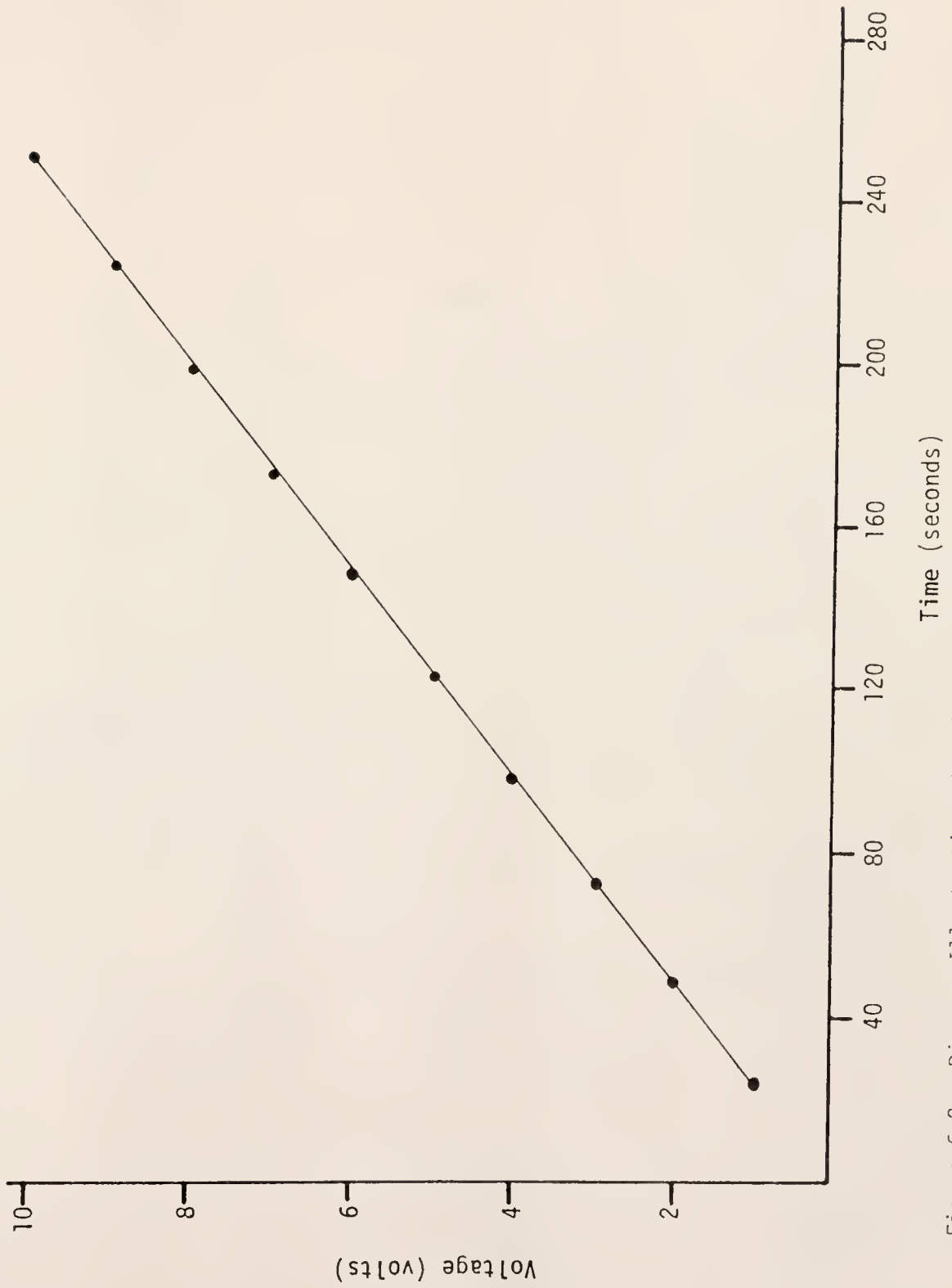
Figure 6.2. Diagram Illustrating the Linear Response of the Electrometer Amplifier.

Electrometer Amplifier Controlling Circuitry

As previously mentioned, at the beginning of a traverse, a ramping sequence accelerates the transverse mechanism then maintains a constant speed and at the end of the traverse decelerates the mechanism to a stop. The repetetive integral method integrates the detector signal over a period of time; however, the data required by the reconstruction algorithm are the transmission data versus transverse distance. The graph of distance versus time, Figure 6.3, shows that the only period during which time and distance traveled are proportional is during the constant speed section of the traverse. It is therefore important to accumulate data only in the time interval between the end of the acceleration and the beginning of the deceleration.

The data recording system chosen was an IBM compatible nine track tape recorder. The recording system electronics is a complete system except for the electrometer amplifier. It requires only four signals to process data placed on its input lines. These pulses are a clock pulse, a pulse to trigger the first reading sequence, a pulse to trigger the second reading sequence, and a pulse to trigger the shift registers, which in turn transfer the data to magnetic tape, (Fitzgerald 1974).

The electrometer amplifier circuit, Figure 6.4, controls the amplifier cycle, prevents data from being taken during accelerations, and sends the appropriate signals to the recording system. The circuit receives pulses identical to those sent to the motor driver boards and operates on a 64 pulse cycle.

Counters B and C of Figure 6.4 have been left in their reset state, all outputs low, by the general reset pulse supplied by the SCR Figure
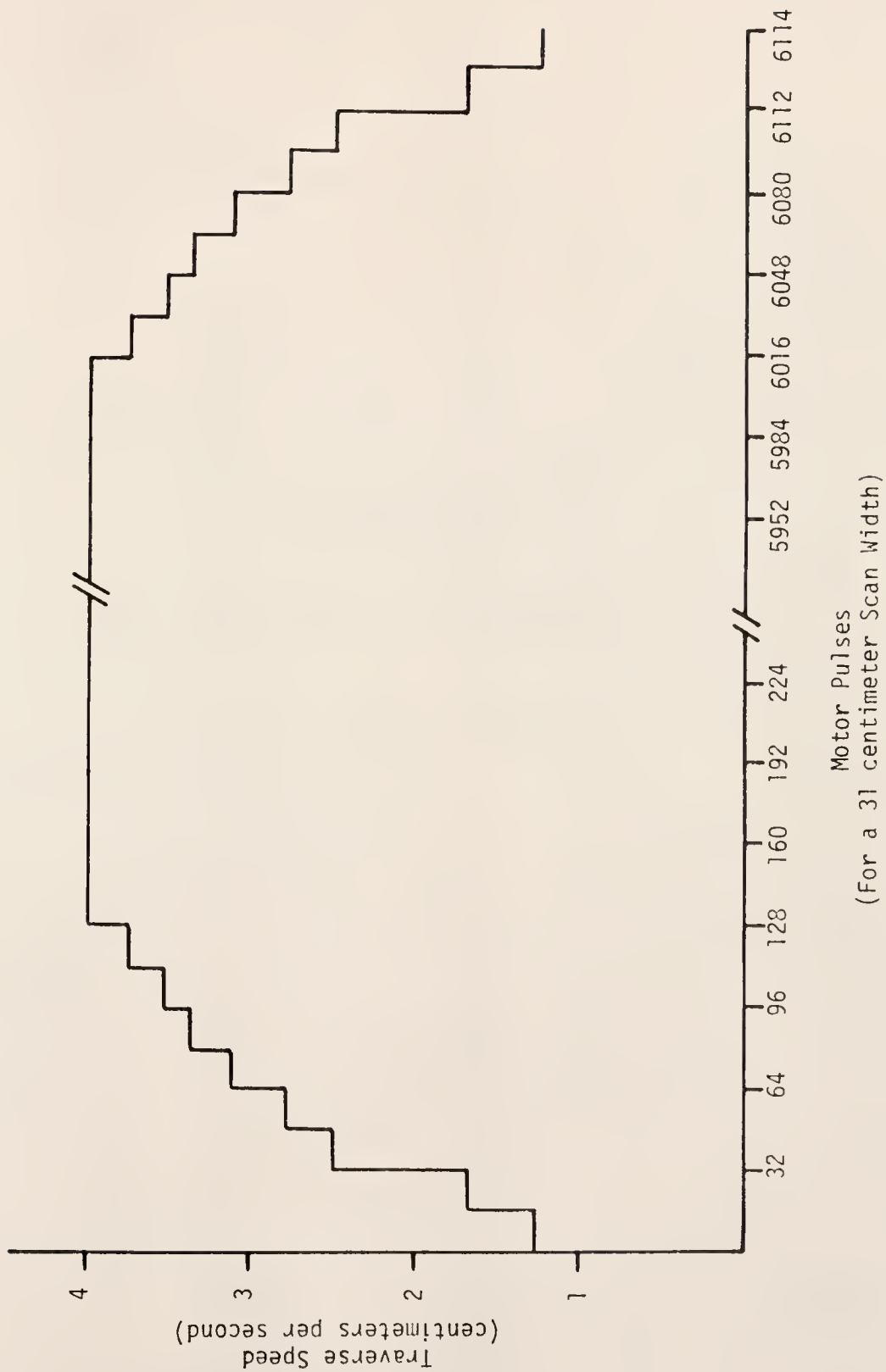
72

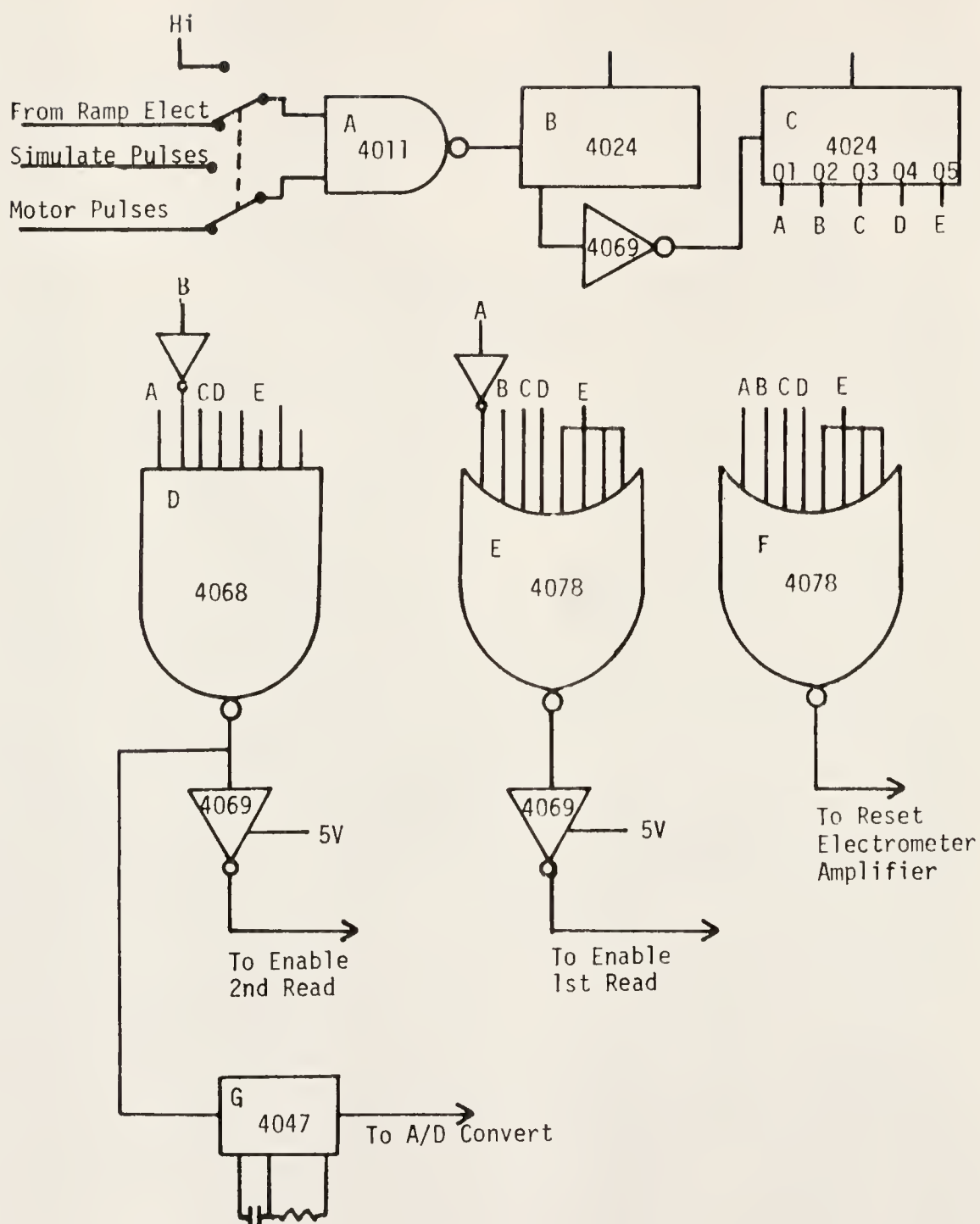Figure 6.3. Diagram of Accumulated Motor Pulses Versus Transverse Speed.

Figure 6.4. Diagram of Electrometer Amplifier Controlling Circuit.

5.2.   The pulses to the circuit enter via switch S1, which for scan-
ning is in the position shown. The alternate function of the switch
is to allow the amplifier to be cycled during the scanner setup, to
allow adjustment of the amplifier gain. While the traverse mechanism
is being brought up to speed, gate A is inhibited by the input from the
ramping electronics. Once full speed is reached, this input goes high
allowing gate A to pass pulses to counter B and in turn counter C. At
the trailing edge of the first motor pulse, Q_1 of counter C goes high,
bringing gate F low, thus bringing the electrometer amplifier out of
reset. The current from the photomultiplier tube is accumulated and after
the third motor pulse the first read sequence is triggered by gate E going
low. The amplifier is then allowed to accumulate current until the
59th pulse at which time gate D goes high and triggers the second read.
The electronics within the recording system subtracts these two values
and stores the difference. This pulse also initiates a sequence which
shifts the data to the recording equipment where it is recorded on a
nine track magnetic tape. The 63rd motor pulse brings counter C outputs
to all zero and the 65th pulse begins the second measurement cycle. The
number of cycles in a traverse is dependent upon the scan width chosen.
The 40 centimeter scan has 128, the 30 centimeter width has 92, and the
20 centimeter width has 64. Although the number of intervals change,
the distance traversed during each measuring interval remains constant,
being determined by the mechanical design of the traverse system. The
motors require 24 pulses per rotation, the gear reduction units are
ten to one ratios, and the lead of the ball screw is one-half inch per
revolution. It can therefore be calculated that 64 motor pulses move
the source and detector 3.387 millimeters.

CHAPTER 7

SYSTEM PERFORMANCE

The accuracy of the axial tomographic scans made by this system is dependent upon:

1) each traverse being executed with source and detector correctly responding to each stepping motor's command,

2) the alignment of the source and detector in all planes, and,

3) the accurate detection and recording of the radiation transmission profile by the data acquisition system.

The tests required to verify if either the source or detector have mistepped during a traverse was straightforward. In using two stepping motors to drive the source, a situation is created whereby both motors must perform flawlessly, since a missed step in either or both motors will result in the loss of driving torque. By marking the starting point of the source's first traverse, a check can be made confirming that at the end of every second traverse the source returns to the same position. This procedure was followed with the source and detector traversing in the vertical direction, the condition of maximum motor loading. In order to determine that the controlling electronics were working correctly, a pulse counter was used to monitor the pulses sent to the motor. Dozens of traverses were made at this

75

orientation and in every second traverse the source and detector
returned to the same initial reference point indicating accurate
mechanical movement by the stepping motors. The number of pulses sent
to the motors for each traverse were also identical. It was felt
that,in order to verify the alignment of the source and detector in all
planes, the output of the detector system would be the most sensitive
and reliable test possible. The rotational system was held fixed with
the source and detector traversing horizontally and the signal over
several traverses was recorded. Significant variations in the detected
beam intensity were found. Upon further investigations using an optical
system showed a misalignment in a plane perpendicular to the face of
the main rotational drum. An attempt to correct this situation was made
by shimming the support shafts, but further scans involving rotation
as well as translation surfaced two other system characteristics
which caused inconsistency in data collection. The first was an abrupt
change in beam intensity occuring several times per scan at angular
orientations between plus or minus 45° to the horizontal traverse.
These changes occured only during rotation and not translation and
were attributed to a shift of the source inside its seated capsule.
The second system characteristic was a variation in transverse align-
ment of source and detector at different angular orientations.

The above inaccuracies were too large to simply ignore; therefore,
a mathematical correction was investigated. Since the objects to be
scanned should never completely fill the transversing distance
there should always be unattenuated transmission values at the edge of
each transmission profile. This coupled with the fact that the variations
in alignment during rotation were consistent from scan to scan and that
the abrupt shift of intensity occurred only during rotation enabled a
simple algorithm to be formulated.

The algorithm first requires a scan with no object in the beam to accumulate the alignment data. It then creates a set of normalization factors which when applied to the raw transmission data yields a transverse scan corrected free from misalignment errors. Compensation is not made for the abrupt change in intensity.

The reconstruction algorithm requires that the unattenuated value of the beam be known at each transmission measurement position. Since the actual transmission data has been corrected, any unattenuated value could be used as the value for Io. As previously stated, the first and last few transmission measurements are always free of attenuating material and therefore can be used to calculate the fractional transmission for their particular traverse. By calculating the transmission in this manner, changes in intensity during rotation can be ignored.

Data Acquisition System Performance

After the mechanical scanning system was aligned the reproducibility and linearity of the data acquisition system were determined. These were first examined by viewing multiple integrating cycles and examining the electrometer amplifier output voltage versus time. Figure 7.1 shows the voltage versus time relationship for a number of integrating cycles with the source and detector stationary and a negative 500 volts across the photomultiplier tube. Both reproducibility and linearity of the measurements can be seen. This test was repeated after increasing the photomultiplier tube voltage to 600 volts, Figure 7.2. The only noticeable difference in the two is the increase of the amplifier output voltage due to higher detector current.

When NaI(Tl) crystals are heavily pulsed they exhibit an afterglow effect. In order to verify that the level of radiation is high enough
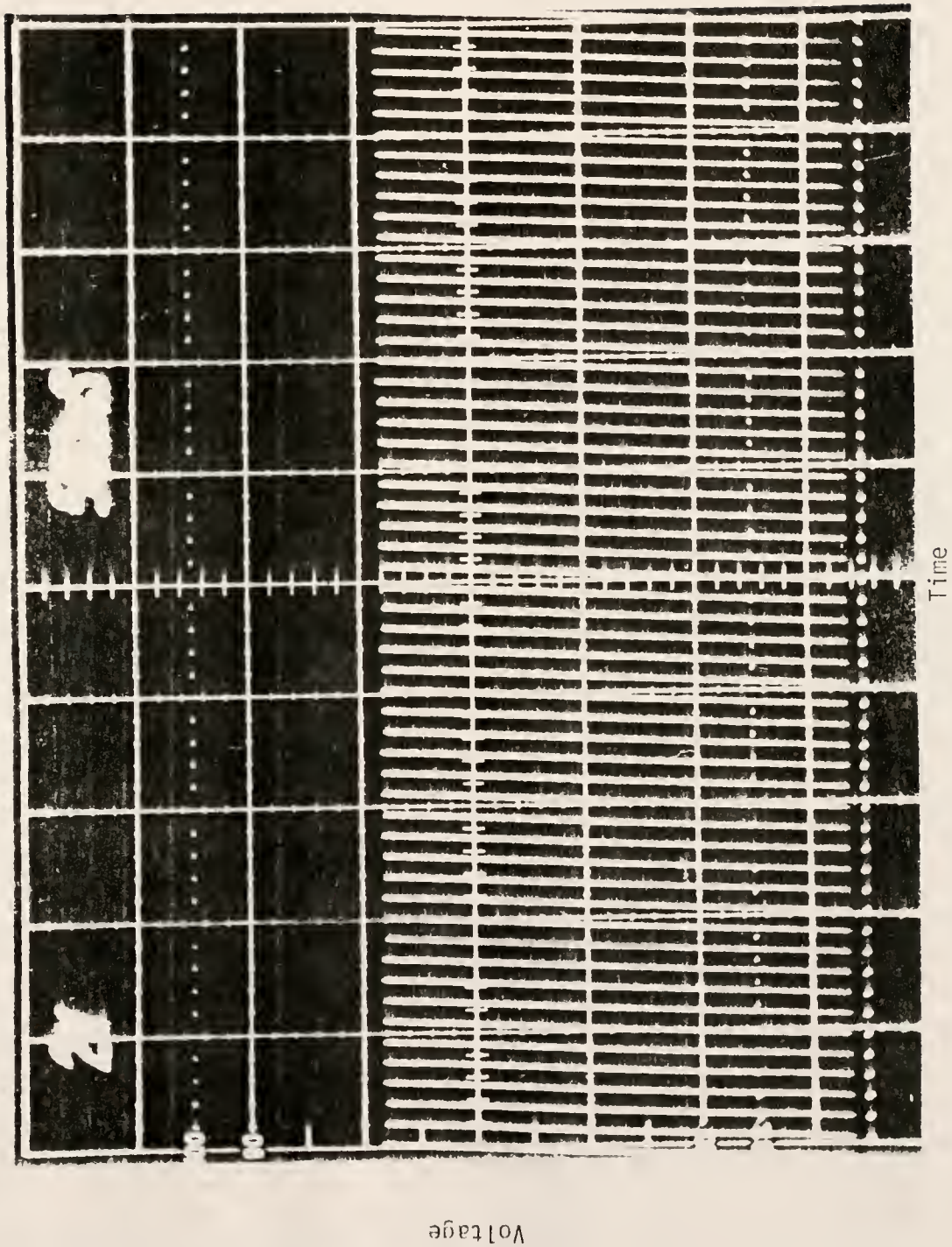
Time

Voltage

Figure 7.1. Response of Detector System with 500 Volts across the PM Tube.
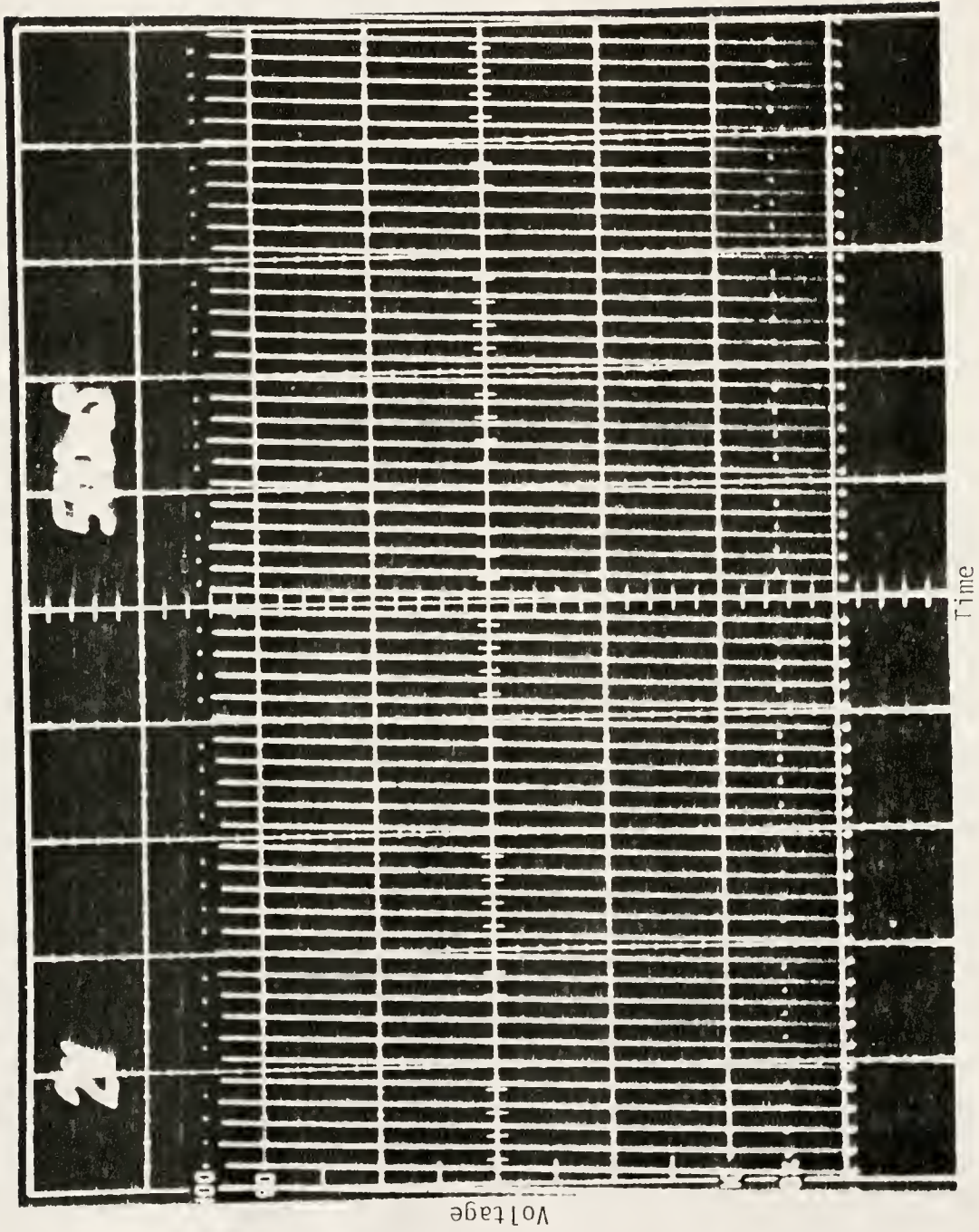
79

Figure 7.2. Response of Detector System with 600 Volts across the PM Tube.

to cause this effect and to quantify perturbation it would have on
the data, further experimentation was required. The effect was first
examined by quickly moving the radiation source to the off position,
with a negative 500 volt across the photomultiplier tube. The first four
integrating cycles of Figure 7.3 were the result of the source in the
on position. During the fifth cycle, the source was quickly moved to
the off position. If there was not an afterglow effect the amplifier
voltage should stay at the value it had obtained when the radiation beam
was interrupted. This, however, was not the case and the voltage con-
tinued to increase. The afterglow current can continue to be observed
in the integration of the next few cycles. To determine if this effect
was at all dependent upon photomultiplier tube voltage, the experiment
was repeated with a negative 980 volts applied to the photomultiplier
tube. These results can be seen in Figure 7.4 and are identical to those
of Figure 7.3, demonstrating the effect is actually a crystal phenomenon.

Although the afterglow effect could be demonstrated by complete loss
of radiation signal, the effect that it would have on the transmission data
during the scanning procedure had to be determined. Figure 7.6 shows the
effect of three millimeters of lead being placed in the beam between the
fifth and sixth integrating cycles. A slight afterglow effect may be
present on the seventh cycle, but from the eighth cycle on, the small
variation in signal can be attributed to the lead not being held steadily
in the beam. This amount of lead inserted into the beam represents a step
reduction of beam intensity of approximately 15%, a step response of the
magnitude that could typically be encountered during scanning. From these
results, the response of the detector system can not be termed ideal, but
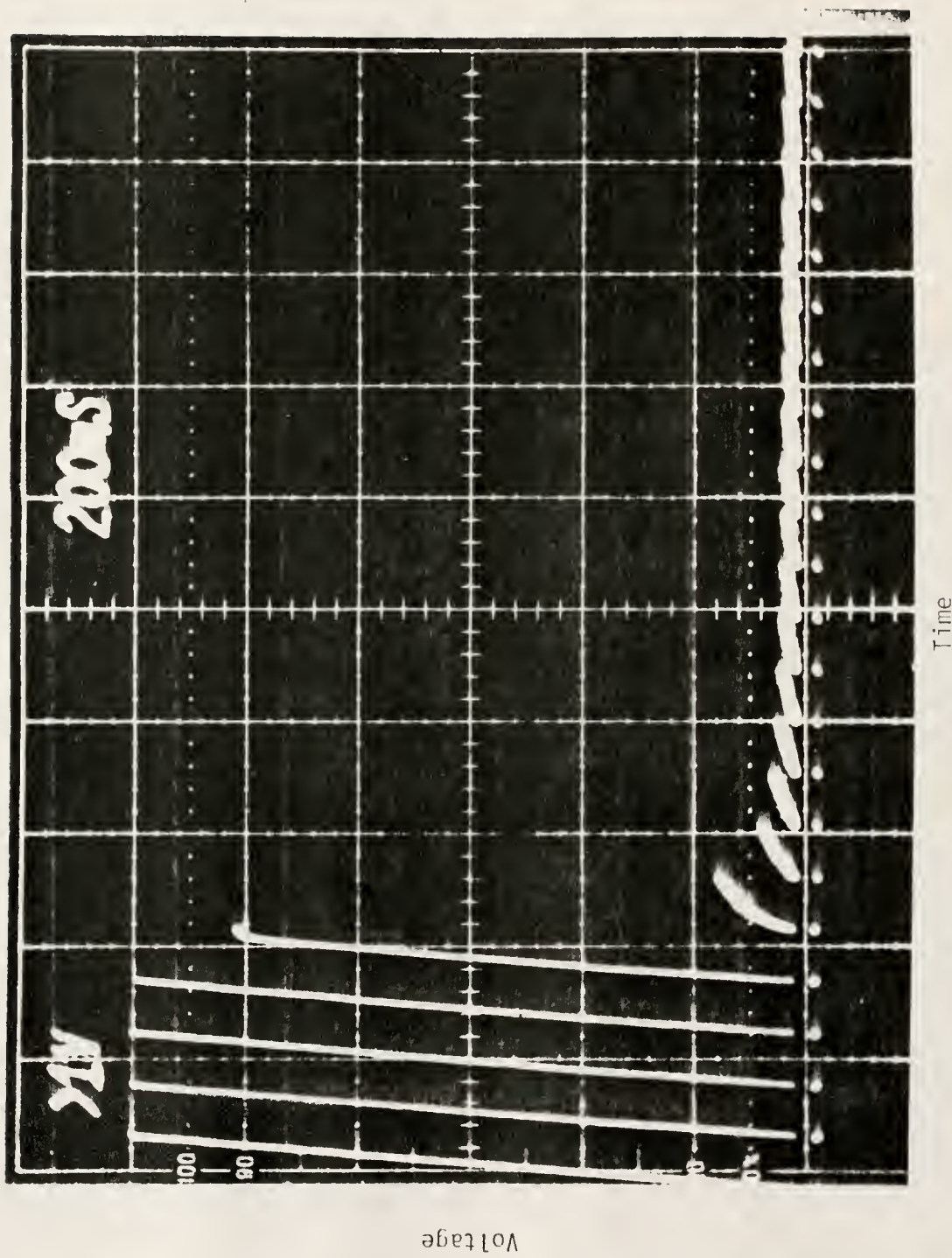it can be termed satisfactory.

Time

Figure 7.3. Response to Step Loss of Radiation with 500 Volts across PM Tube.
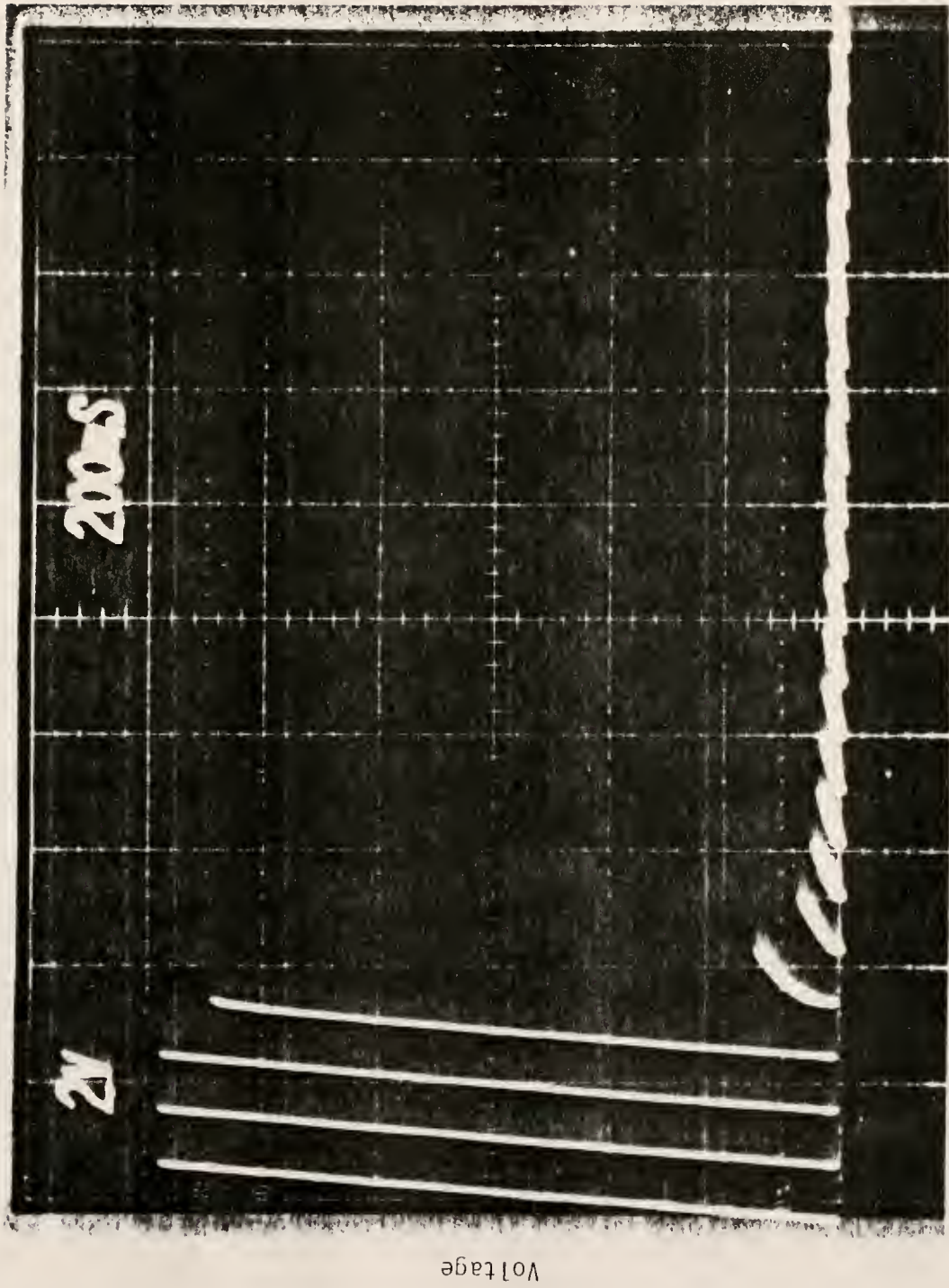
Voltage

Figure 7.4. Response to Step Loss of Radiation with 980 Volts across PM Tube.
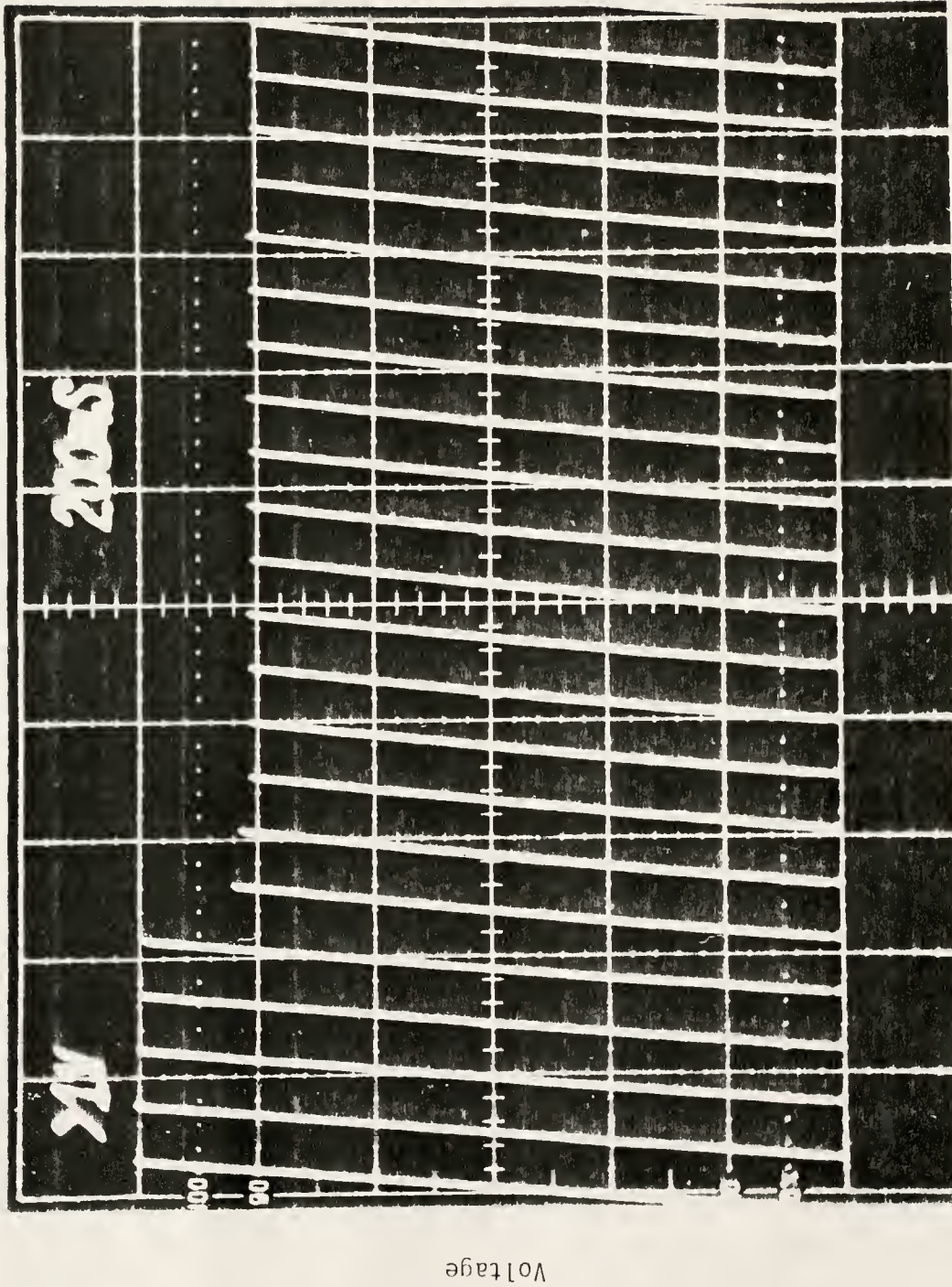
83

Figure 7.5. Response to a Small Negative Step of Beam Intensity.

The next step was to determine the effect during transverse scanning with the rotational system locked at one angular orientation. The first transverse scan was performed to test the response of the system to a large step change of beam intensity. In order to obtain this beam profile, a four inch by four inch lead brick was placed in the scan path. The results can be seen in Figure 7.6. The abscissa is incremented in intervals of integration and the ordinate incremented in the logarithm of transmission. The asterisks indicate the values scanning right to left while x marks the points for the left to right scan. During a left to right scan, the edge of the lead brick is first encountered during the sixth integration interval and by the eighth interval the detector system has equilibrated to the decreased radiation level, results predicted by Fitzgerald (1974). On the thirty-seventh interval, the beam emerges from the brick and the increase in beam intensity is encountered. When scanning from the opposite direction the difference in the transmission values between the asterisks and xs can be seen. At the abscissa point marked as the sixth integration cycle the xs are measuring a decrease in radiation signal while the asterisks are measuring an increase. The afterglow phenomenon causes the xs not to equilibrate to the decreasing beam condition as quickly as the asterisks show the response to an increasing beam. On the opposite side of the brick, at the abscissa value of 37, the xs are measuring the increasing field while the asterisks are measuring the decreasing field, the same effect is seen. It is significant to notice that the correct values were always obtained by the first full cycle after the step function was encountered.

Although such a large step function allows the effect to be dramati-cally demonstrated, it does not reflect the real scanning situation.
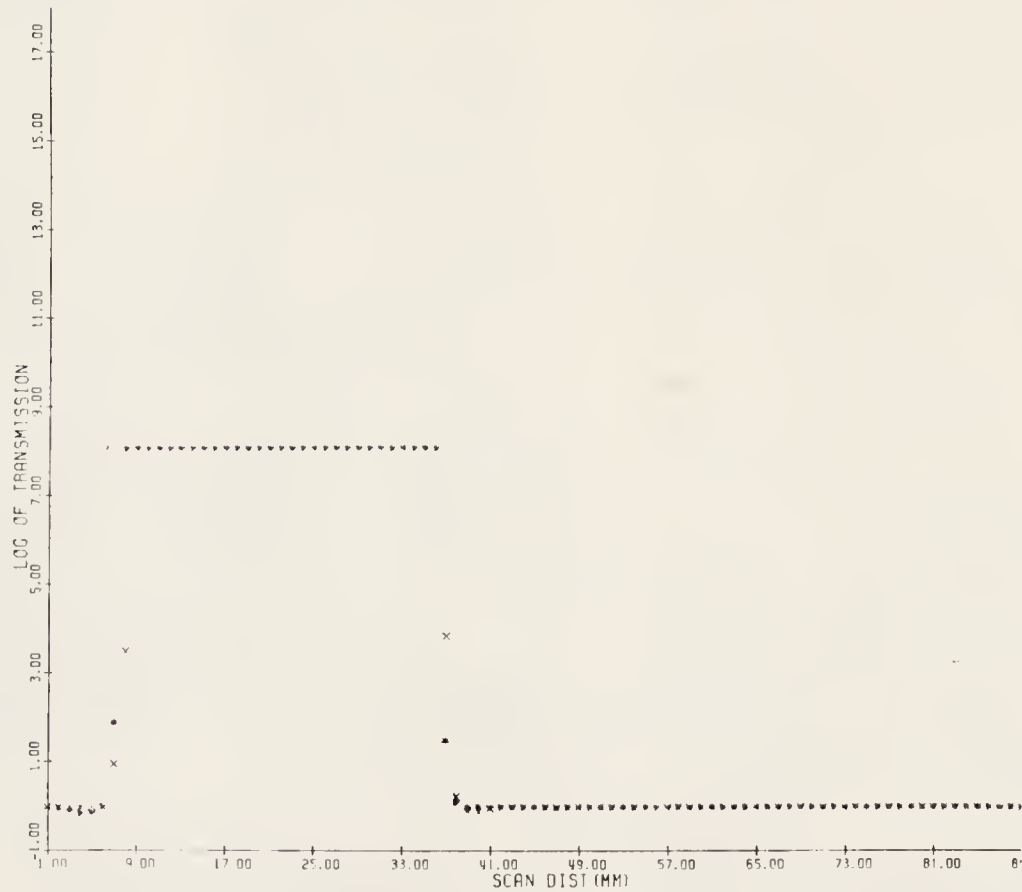
Figure 7.6.   Data System Response to a Lead Brick in the Traverse Path.

To simulate the effect which could be expected during a routine scan, a six inch diameter Lucite cylinder was scanned in the same manner as the lead brick. Once again the shift in data can be seen in Figure 7.7 with the xs and asterisks leading and lagging each other during the same corresponding beam situations. This shift can more easily be seen in Figure 7.8 in which the xs have been replaced by a solid line and the asterisks by diamond shaped symbols. The symbol which is following the decreasing field always lags the symbol measuring the increasing field.

A third experiment performed with a smaller Lucite cylinder, is shown in Figure 7.9. This cylinder being of a smaller diameter caused the radiation intensity gradients to be steeper, but after examining the data, it was found that the deviations due to the afterglow effect were similar in magnitude to those of the larger cylinder. In examining the two sets of data, the smaller cylinder may appear to have much larger deviations, but this is a result of the change in ordinate scaleing.

Finally, the question of whether the afterglow effect would mask small changes in beam intensity was examined. Five Lucite rods, with diameters of 6.5 centimeters, 2.8 centimeters, 1.7 centimeters, 1.0 centimeters, and 0.67 centimeters were placed in the scan path. The results of two scan passes, from the same direction, are shown in Figure 7.10. The measuring system, taking data on the 3.3 millimeter grid, adequately detected and measured the transmission through even the smallest cylinder. The data also demonstrates the reproducibility of the recorded transmission values for each rod.

The evaluation of the overall system shows the presence of the afterglow effect due to the NaI(Tl) crystal being pulsed at a high rate. Although the effect can be readily demonstrated, it amounts to
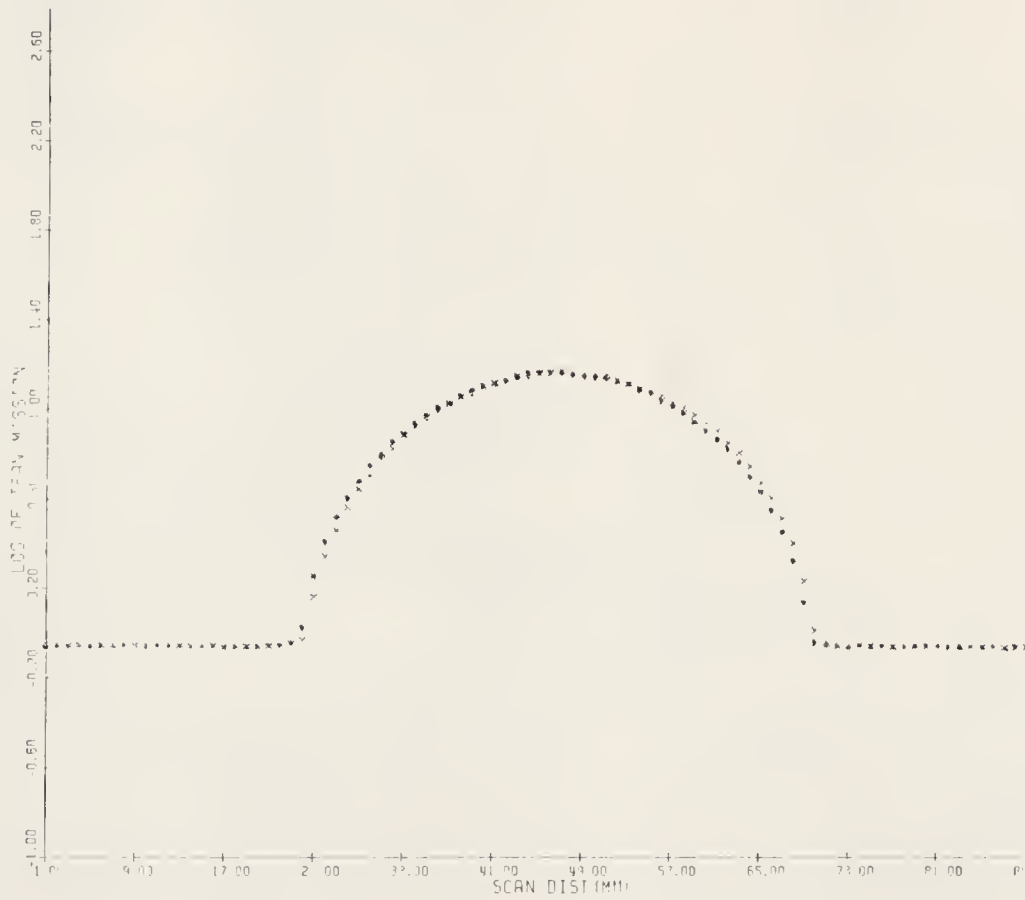
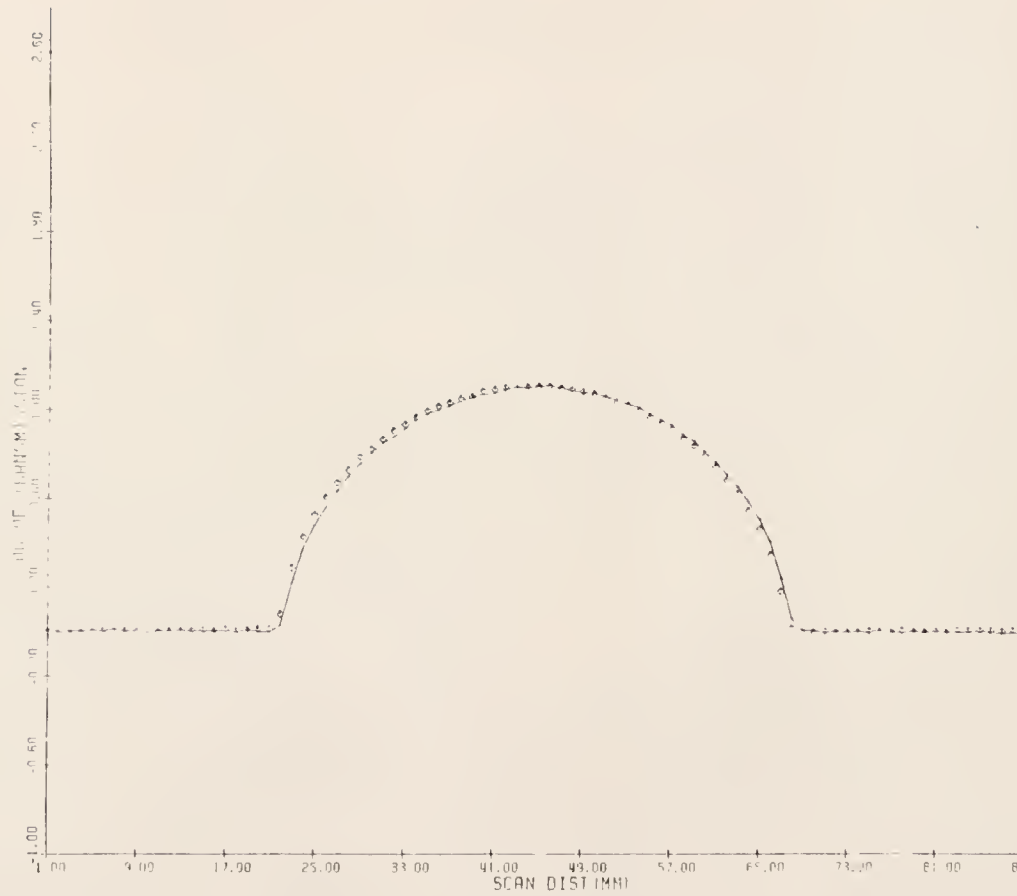Figure 7.7.   Data System Response to a Cylinder in the Traverse Path.

Figure 7.8.   Data System Response to a Cylinder in the Traverse Path.
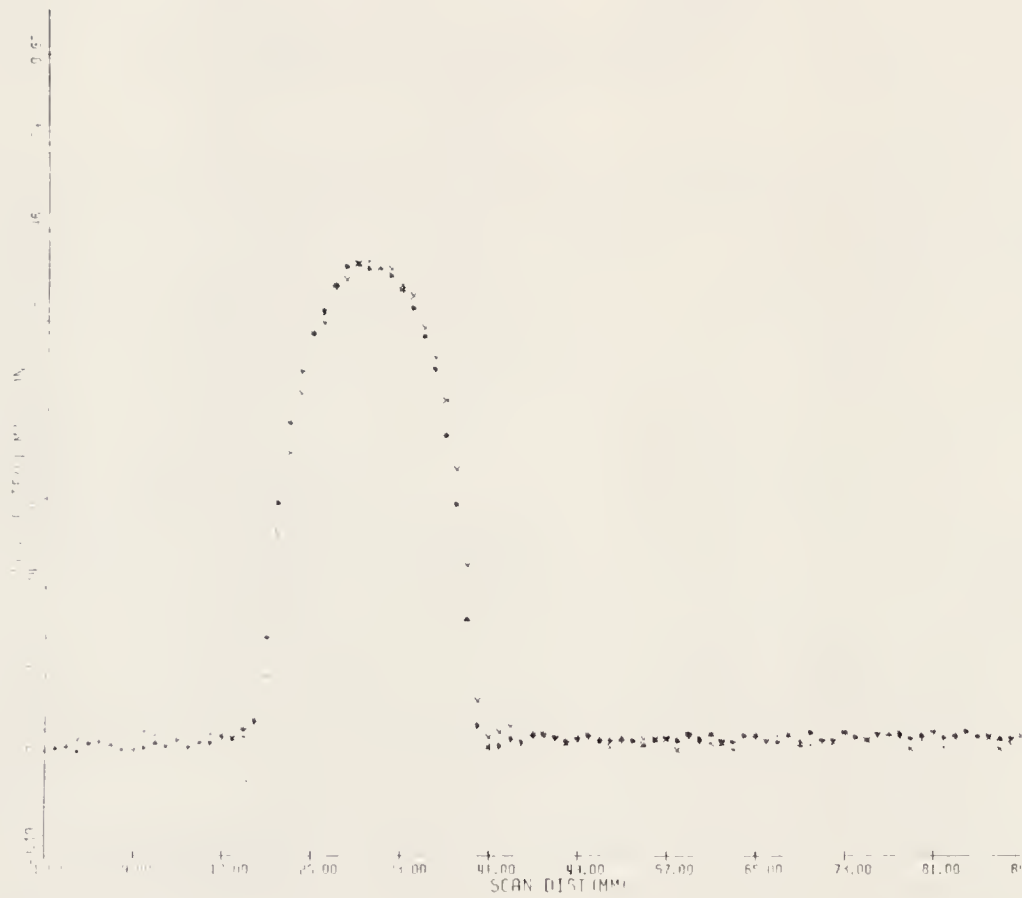
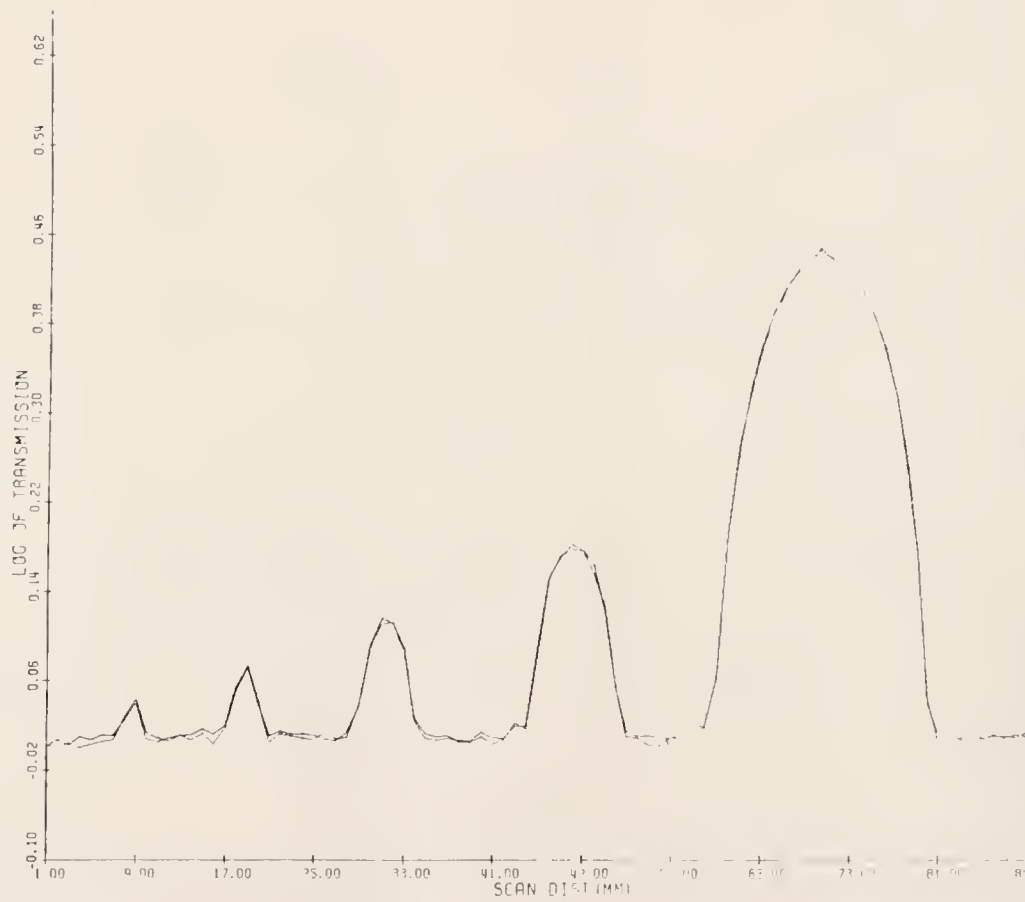Figure 7.9.   Data System Response to a 6.5 centimeter Cylinder.

Figure 7.10. Data System Response to Cylinders of Varying Diameters.

less than 1% during normal scanning situations. It is also of inter-
est to note that if a curve is fit to the transmission data, these
inaccuracies are reduced. It was therefore decided to continue this
detector system and subject alternate detection systems to similar
testing at a later time.

Reconstruction Grid

The first test of the system as a whole was the scan and recon-
struction of a solid Lucite cylinder. This demonstrated the system's
ability to reconstruct a homogeneous volume with an attenuation coef-
ficient close to that of normal tissue.

For this first scan, as in all subsequent scans, the photomultiplier
tube voltage of negative 600 volts was used. The transmission data were
collected on a 3.38 millimeter, 92 by 92 member, grid with 36 evenly
spaced angular views taken.

When these data were reconstructed, it is obvious from the poor
results that 36 views is too few to specify a unique solution for a
92 by 92 member matrix. If the total number of data points do not
equal the number of reconstruction points, the data will not have the
independence required for a unique solution.

Many of the reconstruction methods can, however, produce a matrix,
even if the proper number of data points are not taken. The results
of such reconstruction generally shows large statistical fluctuations
through homogeneous areas and overall inaccuracies throughout the entire
reconstruction.

If a matrix of n by n pixels is to be reconstructed the total
number of valid reconstructed points will be approximately $n^2\pi/4$.
If each scan ray contained n transmission measurements then $n\pi/4$ views

would be required. Since the time limitation imposed on a scan permitted only 36 views to be taken, it was decided to interpolate a 49 by 49 member grid, which produced data on a one-quarter inch matrix. This new transmission data set was interpolated from the original transmission data collected.

In comparing a reconstruction of the 92 by 92 member grid with that of the 49 by 49 member grid, both being calculated from the same raw data, the latter produced a more uniform and accurate image. All subsequent scans were therefore reconstructed on the one-quarter inch grid system.

The reconstruction of the Lucite cylinder is shown in Figure 7.11. The superimposed grid outlines the area around each pixel with its value being right justified to the pixel center. There is also an approximate outline of the cylinder and a triangle to mark the center of the reconstruction grid. It can be seen that the cylinder was placed in the lower left quadrant which yields a worst case situation, since the area for accurate reconstruction is only within a radius of n from the center of the grid.

The mean reconstructed value for the cylinder is 68, the actual value obtained multiplied by 1000, with a standard deviation of two. The variation of the values at the edges of the object is a result of the pixel being only partially within the cylinder.

This is simply an artifact produced by the spatial resolution of the grid as it tries to follow a step function, the smaller the pixels are, the more accurately the step function can be followed.

The decreased accuracy toward the bottom and lower right sides of the cylinder may be caused by its position within the scan grid. A small amount of this effect may be due to the outline of the
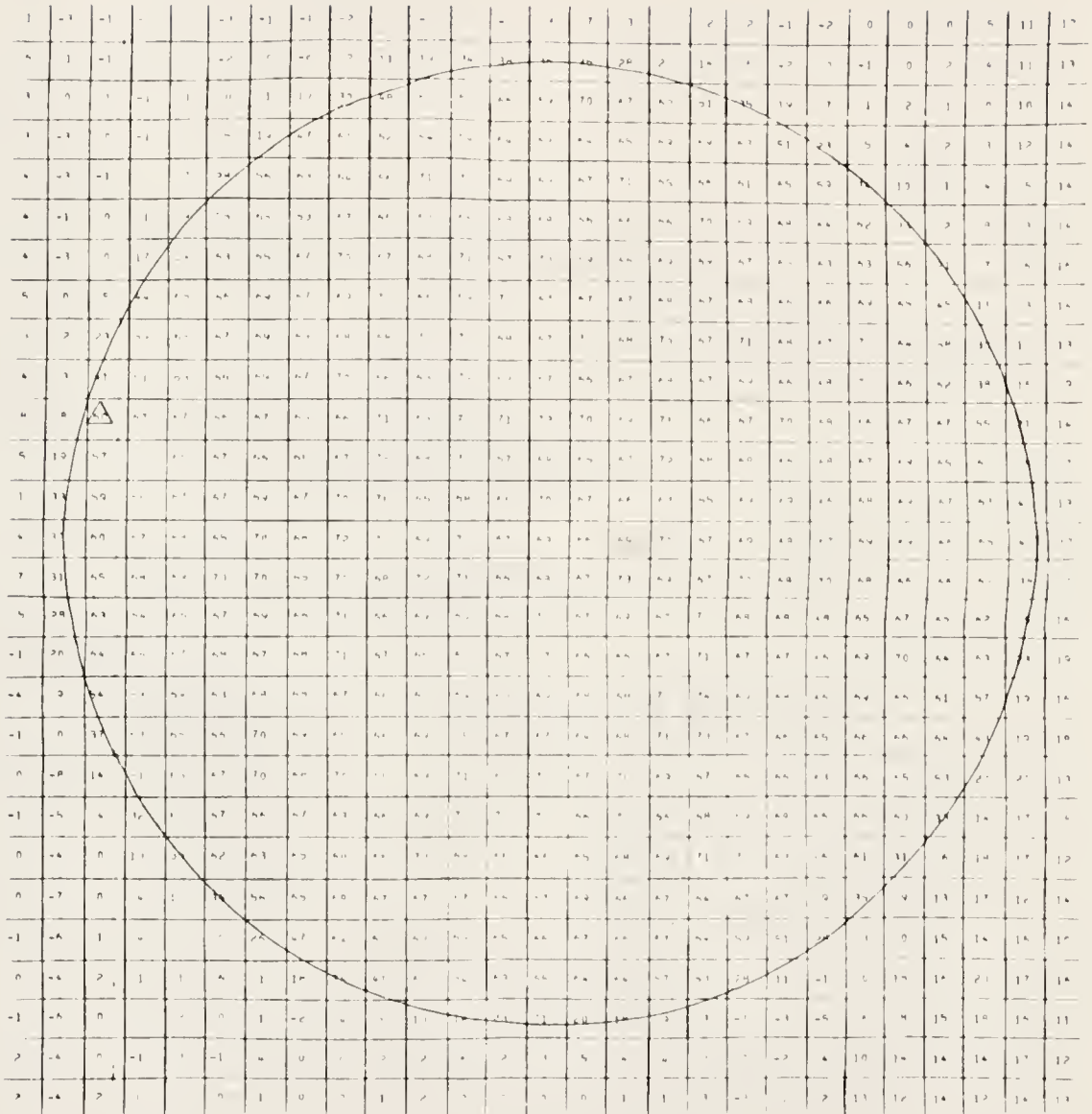
Figure 7.11.   Reconstruction of Lucite Cylinder.

cylinder being slightly mispositioned on the computer output. In either case, the edge effect is a real effect and will be present in all discrete images of this type. Overall, the reconstruction of the cylinder demonstrates the ability of the mechanical system and data collection systems to produce a uniform scan even under poor conditions.

The next object chosen to be scanned was a water-filled abdominal phantom. The detector settings, data correction method,and data inter-polations were identified as in the previous scan. The outline of the phontom was not a regular geometric shape and proved to be more diffi-cult to superimpose on the reconstructed matrix. Instead of obtaining the shape and fitting it to the data, a reconstructed value was chosen and an isoattenuation line was drawn. This value, chosen after exam-ining several scans, was 40.

Figure 7.12 shows the reconstructed grid with an isoattenuation curve superimposed. This curve agreed well with the actual phantom shape. The right side of the reconstruction shows an indentation over the lumbar spine with other areas demonstrating reproductions of the phantom sides and abdominal sections.

The third scan was of a head section of the Rando Phantom. The reconstruction can be seen in Figure 7.13 while an x-ray of the section scanned and a side view of the section can be seen in Figure 7.14.

It should first be mentioned that the contour of the phantom was accurately reproduced and that the center of the phantom did reconstruct to the correct value for normal muscle, 63. The bone is also clearly visible in Figure 7.13 (i.e. the higher attenuation numbers) and an isoattenuation line of approximately 69 is shown by the dotted line within the contour. This also agrees very well with the x-ray of Figure 7.14. An interesting effect is seen toward the edge of the
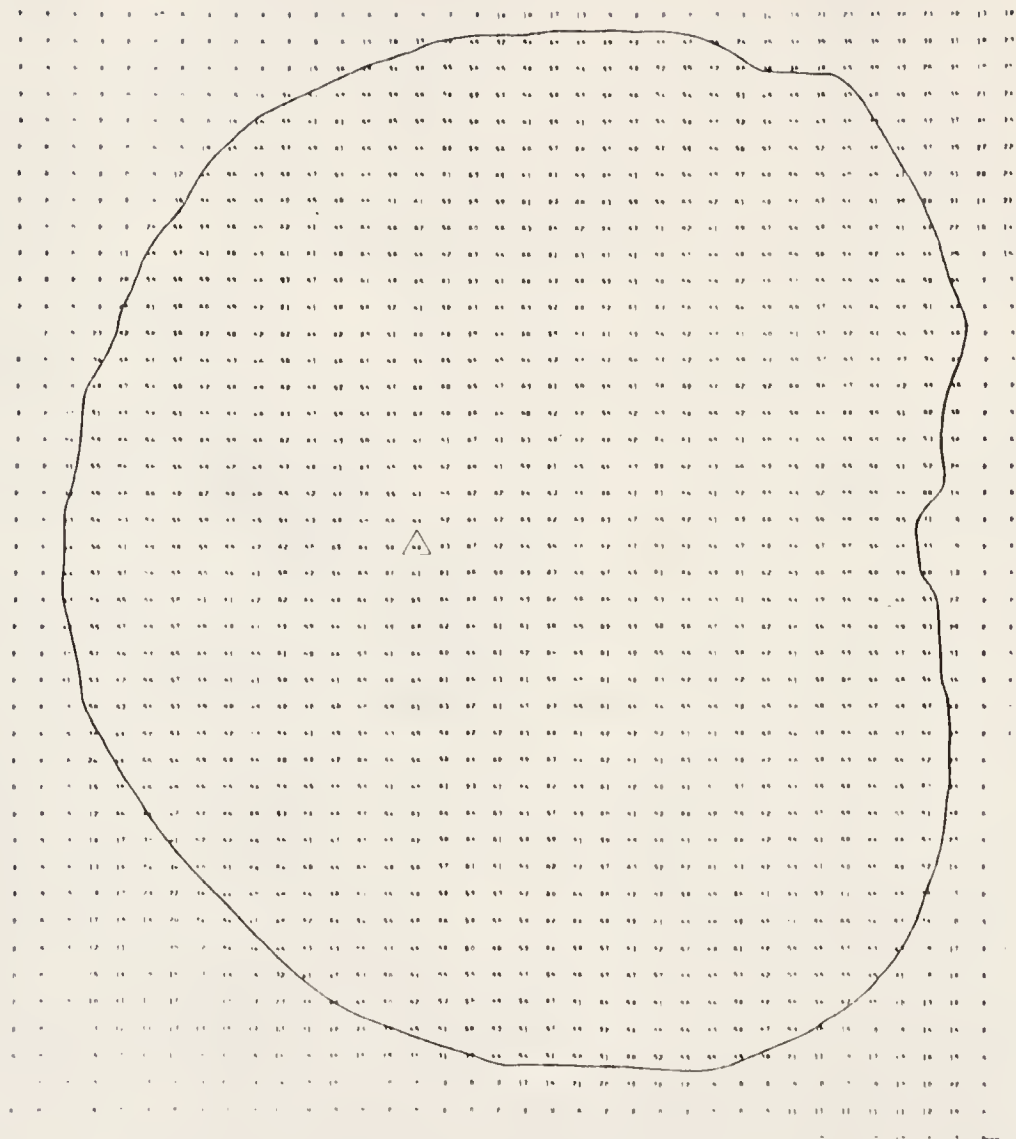
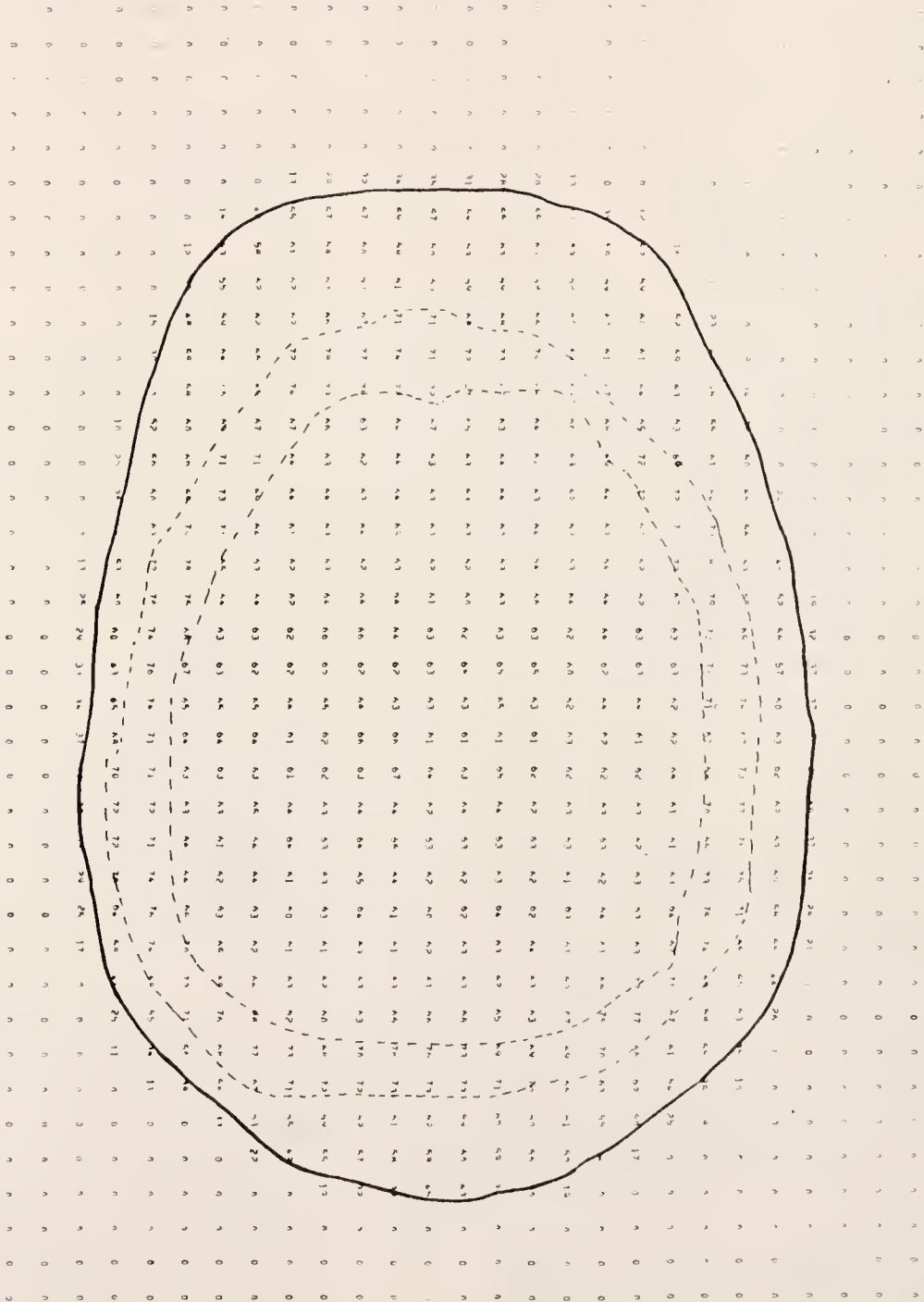Figure 7.12. Reconstruction of a Water Phantom.

Figure 7.13.   Reconstruction of Rando Head Section.

Figure 7.14. Side View and X-ray of Scanned Rando Section.

contour. The values reconstructed seem lower than they should. It would be expected that these values would be equal to those for soft tissue, which is 63, but instead range in the high 50s. The reason for this can be seen by examining the side view of the phantom in Figure 7.14. The values reconstructed are for pixels positioned trans- axially, however, the slope of the contour causes these pixels to be positioned only partially inside the phantom. This in turn caused the reconstructed attenuation value to be low.

To demonstrate the reproducibility of the system, a second scan was done of the same phantom section, Figure 7.15. The reconstruction is nearly identical with reconstructed values within statistical fluc- tuations. Since the microswitch positioning the system was not used during setup for these scans, the small differences in reconstructed values could have come from a small shift in position of the phantom relative to the scanner.

The fourth scan is that of another head section of a Rando Phantom. The reconstruction is shown in Figure 7.16 and the x-ray of the section in Figure 7.17. Once again the 40 isoattenuation line correctly out- lines the contour with the nose and ears closely outlined.

The correlation between Figure 7.16 and 7.17 is difficult since the reconstruction is of only a one-half centimeter slice through the 2.54 centimeter section radiographed. It also appears that the scan was performed with the left side being more inferior than the right, causing the sinus cavity to only be visible at the right side.

The reconstructed images shown demonstrate the ability of the scanning system to accurately reproduce scanned objects. Good agree- ment was obtained for the values of soft tissue and bone and the system's ability to accurately determine the contour of the object by
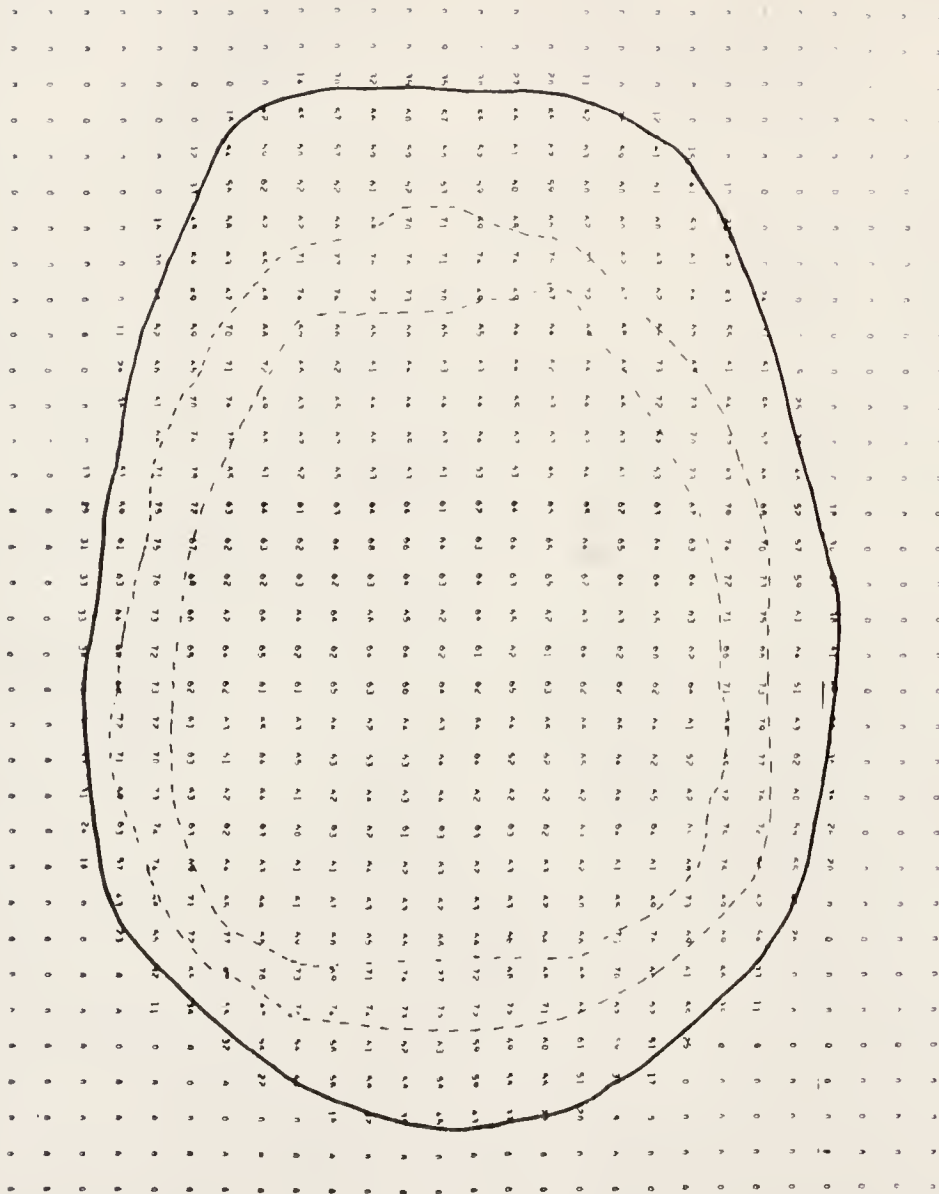
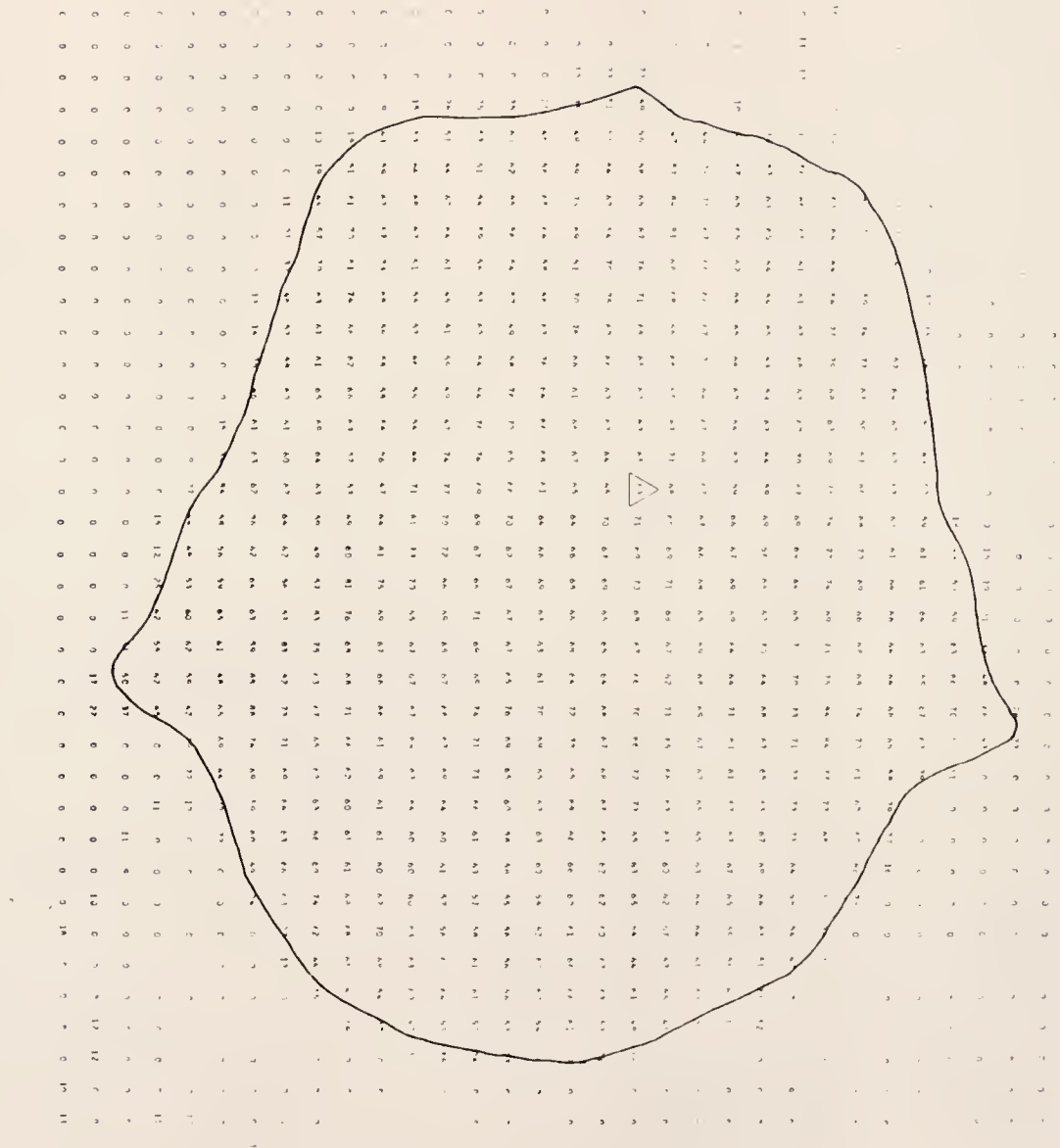Figure 7.15.   Repeated Reconstruction of Rando Head Section.

Figure 7.16. Reconstruction of Rando Head Section.

Figure 7.17.   X-ray of Rando Head Section.

following an isoattenuation line was demonstrated. The inaccuracies demonstrated by the data acquisition system during testing did not seem to significantly effect the data.

Treatment Planning Algorithm

The utilization of the reconstruction data is dependent upon an accurate and easily implemented treatment planning algorithm. This algorithm must incorporate the following steps:

1) obtain a subject contour,

2) position the isodose fields relative to the contour,

3) the transfer of the reconstructed scan matrix to the treatment planning algorithm,

4) correct the isodose curves for oblique entry, and

5) correct the isodose curves for inhomogeneity with the contour.

The transfer of the data is very simply performed. As previously mentioned, the scan data are recorded on a nine track magnetic tape which is transferred to a time-sharing macro-computer. This is the same computing system that is used for the execution of the treatment planning algorithm. The transfer can be achieved by storing the reconstructed matrix in a data set to be later retrieved by the treatment planning program or the two programs can be linked together and the data set simply passed from one to the other. In either case, the data are readily available and the method of transfer is a matter of programmer preference.

Obtaining the patient contour is not as simple a matter. It seems that the best approach is to always try to center the scanned section about the center of the scanning matrix or at least have the center of the matrix lie within the scanned subject. Once this has been achieved, at a number of preset angular orientations the gradient of attenuation coefficients, from the center outward, can be determined. When a steep negative gradient is encountered with the values beyond consistently near zero, it can be assumed that the edge of the contour has been found. This procedure would be carried out until enough angular orientations had been obtained to adequately define the contour. Past experience with the treatment planning algorithm presently in use indicated that the number of orientations would be 36.

An alternate method, which has been demonstrated, is to simply pick an isoattenuation line to outline the object. This would adequately define the contour which could then be superimposed on the coordinate system required by the treatment planning algorithm.

The positioning of the isodose field relative to the contour is a difficult task. At the present time, it seems as though the contour would have to be produced on hard copy. The fields would then be positioned and located relative to the reconstruction grid. These coordinates would then be fed back into the computer and the treatment planning algorithm then executed.

The present method of correcting isodose curves for oblique entry is by the use of an algorithm written by Fitzgerald (1977). There seems to be no reason to alter this algorithm for it has proven to be a reliable and accurate method of correction.

The correction for inhomogeneity will be incorporated into the present treatment planning program as a single subroutine. The subroutine will correct the data with the following consideration:

1) edge effect Because of the edge effect seen in Figures
7.12 and 7.14 no correction for inhomogeneity will be
attempted for the three-eighths of an inch inside the
contour. In most cases, this area will only contain
skin and the low values encountered will simply be
considered spatial resolution inaccuracies.

2) changes in homogeneity The statistical fluctuations of
the reconstruction must be taken into account when the
data are to be corrected for inhomogeneities. To allow
for these errors a range of normal tissue values of
0.057 to 0.069 will receive no correction. This con-
stitutes a band of plus or minus 10% of the normal tis-
sue value. If after experimentation this is found to
be too large or too small a tolerance, it will be adjusted
accordingly.

3) type of correction The correction performed will only be
for the primary radiation reaching the point being cor-
rected. A correction for its increase or decrease in
absorption will be performed. After investigation of the
accuracy of this approach, a correction for forward scatter
may be added. The problem which must be avoided is
excessive computational time wasted on overzealous cor-
rections beyond required accuracies.

The correction procedure will involve the examination of each
pixel which the dose field encounters as it progresses through the
contour. Figure 7.18 shows a section of a reconstruction with the
reconstruction grid, the value of the pixels, the contour, the posi-
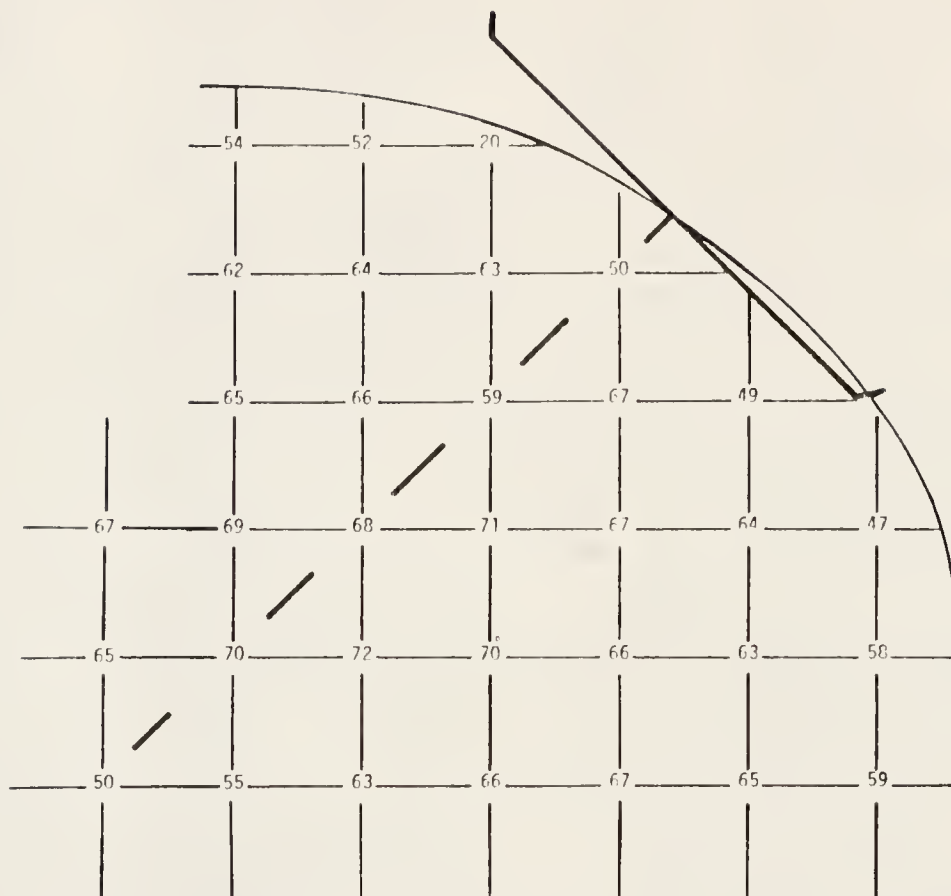
Figure 7.18.   Isodose Curve Position Relative to Reconstruction
               Grid.

tion of the isodose field, and the projection of the central ray within the contour shown.

The first reconstructed point encountered has a value of 0.050, but because the point is not three-eighths of an inch inside the contour, no correction will be made. The next two points encountered by the central ray have values of 0.059 and 0.068 respectively. Since these values are within the band of normal tissue (0.057 to 0.069), no correction of the isodose field will be made.

The next point has a value of 0.070 and will require the isodose field to be corrected. The length of the ray which passes through this pixel and the total absorption over that distance will be calculated. The distance necessary for this amount of absorption through normal tissue, 0.063, will then be computed and the difference between this value and the actual distance traversed will be calculated. A shift of this distance down the ray will be made, and the value at that point will be placed at the isodose point being corrected. An inverse square correction will then be made and the total correction factor stored.

The next point to be reached has a value of 0.050 and a similar correction process will take place. First, the cumulative correction factors for all the preceding pixels will be applied, and then the equivalent distance through normal tissue will be computed. This shift, however, will be in the opposite direction to the previous one, and a value the appropriate distance back along the ray will be moved to the point being corrected with the appropriate inverse square correction then being applied. The total correction up to this point will be calculated, to be used at the next correction point. This process will continue until all the isodose values have been corrected.

Once this process has been carried out for each field entering the contour the resultant dose distributions will have been compensated for oblique entry and anatomical inhomogeneties.

CHAPTER 8

DISCUSSION OF RESULTS

Although the ability to produce accurate and precise axial tomo-
graphic images is the criteria which dictated success or failure for
a scanner, the performance of each of the units sub-systems must be
evaluated so that limitations placed on the overall results can be
realized.

Mechanical System

The mechanical system's ability to continuously traverse, under
maximum load, without loss of motor step, has been demonstrated.
The digital ramping sequence has been shown to successfully reduce the
inertial load placed on the motors, to a level which could reliably be
handled. The precision of the rotational system also has been demon-
strated in the production of accurate axial tomographic images.

Controlling Electronics

The low-cost dedicated digital computer has demonstrated its
ability to control the stepping sequences required for translation
as well as rotation, coordination of the electrometer amplifier cycles
with the constant speed traverse, and synchronization of the data
recording all other systems.

When this system was fabricated, the digital logic was the most reliable type of electronics available, however, the recent advent of moderately priced microprocessors makes available a much higher degree of electronic sophistication at a small increase in cost. Any future designs requiring sophisticated control will examine this new alternative.

Data Acquisition and Recording

The data acquisition system's response to a large step function at photon fluxes on the order of 10^6 photons per second, was judged less than ideal; however, the system does accurately measure and record the transmission profile encountered in routine scanning. A second detector system, which uses a bismuth-germanium-oxide detector, is presently being evaluated. It is hoped that this new system, which is theoretically free of the afterglow phenomenon of NaI(Tl), will more accurately follow the transmission profile and thereby improve the statistics of the reconstructed image.

One of the concerns during development was the possible problems in using a write-only recording system and thereby not being able to immediately verify the scan data, however, the reliability and ease of operation of the system presently in use has removed these concerns. The only changes presently under consideration are to the recording medium to be used. Due to the input restrictions of the time-sharing system, the recording data onto a floppy disc is being investigated.

Scan Time and Pixel Size

The size of the reconstructed pixel, one-quarter of an inch, seems adequate for initial investigation. If, however, this size is judged too coarse for certain areas, such as the head and neck region, the number of views can be increased and the pixel size decreased accordingly. If, on the other hand, the one-quarter inch grid is excessively fine for areas such as the pelvis region, the number of views will be decreased and the pixel size increased.

The scan time, which was increased as the result of the motors being unable to deliver rated torque, is now ten minutes for a head section, 15 minutes for a pelvic section. Further investigation will be made into resolving these torque problems as well as looking into the possibility of a stationary source having a fan beam and a multiple detector arrangement. This latter approach would enable the scan time to be reduced to under one minute.

Utilization of Data

The question which has surfaced, in the evaluation of even the first few scans, is at what level should the axial view be taken to yield a valid representation of the treatment situation. The transaxial sections of Figure 7.14 and 7.16 are only four centimeters apart, yet even with this small separation, the changes in contour and internal structure would cause large differences in internal dose distributions from the same external field arrangement. It can be seen that basing a corrected dose distribution on any one view of internal inhomogeneities, can result in misleading interpretation of the dose throughout the tumor volume.

The objectives of making clinically available accurate and precise data on the position and linear attenuation coefficients of anatomical inhomogeneities has been accomplished and an algorithm for the utilization of these data has been proposed.

An investigation of dose distributions connected with these new data as compared to the distributions previously obtained without inhomogeneity data, will be carried out. It must be realized that in using these new data, we are suddenly attempting to place absolute values on treatment that has been derived through the use of empirical formulas and years of clnical trials.

Attempting to quickly reduce margins around tumors, primarily used because of uncertainties in the dosimetric process, without carefully studying all the implications of such actions can as easily lead to catastrophic clinical results as it can to improved ones.

BIBLIOGRAPHY

Andrews, D. J., "Planigraphy: Introduction and History," Am. J. Roentgenol. Radium Therapy Nucl. Med., 36:575, 1935

Arfken, G., Mathematical Methods for Physics, Academic Press, New York, 1966.

Bentley, R. E. and Inst, A., "Digital Computers in Radiation Treatment Planning," Brit. J. Radiol., 37:748, 1963.

Bloor, R. J. and Quick, R. S., "Treatment Planning in Roentgen Therapy," Am. J. Roentgenol. Radium Therapy Nucl. Med., 76:961, 1954.

Bracewell, R. N., "Strip Integration in Radioastronomy," Aust. J. Phys., 9:198, 1956.

Brooks, R. A. and DiChiro, G., "Principles of Computer Assisted Tomography (CAT) in Radiographic Radioisotopic Imaging," Phys. Med. Biol., 21:689, 1976.

DeRosier, D. and Klug, A., "Reconstruction of Three Dimensional Structures from Electron Micrographs," Nature, 217:130, 1968.

Eichorn, H. S., "Results of Comparative Studies in a Man-like Phantom Between Measured and Computer-Determined Dose Distribution with Different Radiation Methods," Radiology, 88:1154, 1967.

Fitzgerald, L. T., "A Repetetive Integral Measurement Technique for X and Gamma Radiation Dosimetry and Depth Dose Scanning," Doctoral Dissertation, University of Florida (1974).

Fitzgerald, L. T., Personal Communication, 1977.

Gorden, R. and Herman, G. T., "Three-Dimensional Reconstruction from Projections: A review of Algorithms," INT Rev. Cytol., 38:111, 1970.

Hallden, H. I., Ragnhult, N., and Roos, B., "Computer Method for Treatment Planning in External Radiotherapy," Acta Radiol. [Ther], 1:407, 1963.

Hendee, W. R., and Ibbott, G. S., "The Problem of Body Inhomogeneities in Radiation Therapy," App. Radiol., 6:81, 1976.

Hounsfield, G. N., "Computerized Transverse Axial Scanning (Tomography) Part 1, Discussion of System," Brit. J. Radiol., 46:1016, 1973.

Jelden, G. L., Chernak, E. S., Radriquez-Antiunez, Haaga, J. R., Lavik, D. S., "Further Progress in CT Scanning and Computerized Radiation Therapy Treatment Planning," Am. J. Roentgenol., 127:179, 1976.

Ledley, R. S., DiChiro, G., Lussenhop, A. J., and Twigg, H. L., "Computerized Transaxial X-ray Tomography of the Human Body," Science, N.Y., 186:207, 1974.

McCullough, E. C., "Photon Attenuation in Computed Tomography," Med. Phys., 2:307, 1976.

Mauderli, W. and Fitzgerald, L. T., "A Computer Program for Rotational Treatment Planning," Am. J. Roentgenol. Radium Therapy Nucl. Med., 94:810, 1965.

Mauderli, W. and Hazard, B., "Depth Dose Scanning Device," Radiol., 84:130, 1965.

Morgan, R. S., "Structure of Ribosomes of Chomatoid Bodies: Three-Dimensional Fourier Synthesis at Low Resolution," Science, 162:670, 1968.

Olendorf, W. H., "Isolated Flying Spot Detection of Radiodensity Discontinuities - Displaying the Internal Structural Pattern of a Complex Object," I.R.E. Transactions on Bio-Medical Electronics, 8:68, 1961.

Phelps, M. E., Gado, M. H., and Hoffman, E. J., "Correlation of Effective Atomic Number and Electron Density with Attenuation Coefficients Measured with Polychromatic X-rays," Radiology, 117:585, 1975.

Ramachandran, G. N., and Lakshminarayanan, A. V., "Three-Dimensional Reconstruction from Radiographs and Electron Micrographs: Application of Convolutions Instead of Fourier Transforms," Proc. Natl. Acad. Sci. U.S.A., 65:2236, 1971.

Setala, K., "Transfer of Images from Roentgenograms to Transversal Body-Contour Equivalents for Dose Planning in Radiotherapy," Acta. Radiol., 3:361, 1965.

Siler, W. and Laughlin, J. S., "A computer Method for Radiation Treatment Planning," Communication of the Ass. for Computing Machinery, 5:407, 1962.

Skaggs, L. S. and Savic, S. D., "Use of an Analog Computer to Calculate Treatment Dose for Multiple Fields," Radiology, 80:116, 1962.

Sterling, T. D., Perry, M., Katz, L., "Planning Radiation Treatment on the Computer," Annals of the N.Y. Acad. of Sci., 115:976, 1963.

Sterling, T. D., and Perry, M., "Automation of Radiation Treatment Planning (Part IV)," Brit. J. Radiol., 37:544, 1961.

Sterling, T. D., Weinkam, J. J. and Perry, M., "Automation of
    Radiation Treatment Planning V-calculation and Visualization
    of the Total Treatment Volume," Brit. J. Radiol., 38:906, 1965.

Thiem, G. A., Hendee, W. R., Ibbott, G. S., Carson, P. L., and Kirch, D. L.,
    "Cross-Sectional Anatomic Images by Gamma Ray Transmission Scanning,"
    Acta. Radiol., 14:57, 1975.

Tsien, K. C., "The Application of Automatic Computing Machines to
    Radiation Treatment Planning," Brit. J. Radiol., 28:332, 1955.

BIOGRAPHICAL SKETCH

Francis Joseph Bova was born on March 19, 1950, in New York City,
New York. He attended primary and secondary schools of Elmont, New
York, and entered the State University of New York at Farmingdale in
1968. He was graduated in 1970 with an Associates of Science in
engineering science. Mr. Bova then went on to Rensselaer Polytechnic
Institute, Troy, New York, in 1970 and was graduated in 1972 with a
Bachelor of Engineering in bio-medical engineering and again in 1973
with a Master's of Engineering in bio-medical engineering. In 1973 he
entered the University of Florida for graduate work in medical physics.
From 1973 until 1975, he held graduate assistantships and has worked
on projects involving the university's Whole Body Counter, and neutron
activation analysis of trace elements in biological substances.
During this time, he also served as President of the Nuclear Engineering
Society's Student Chapter.

In 1975 he was appointed Assistant in Radiology and has assisted
in clinical physics support and data retrieval systems.

I certify that I have read this study and that in my opinion it conforms to acceptable standards of scholarly presentation and is fully adequate, in scope and quality, as a dissertation for the degree of Doctor of Philosophy.
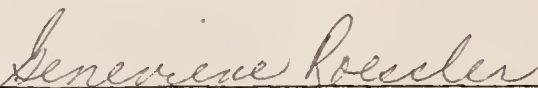
Walter Mauderli, Chairman
Professor of Nuclear
Engineering Sciences

I certify that I have read this study and that in my opinion it conforms to acceptable standards of scholarly presentation and is fully adequate, in scope and quality, as a dissertation for the degree of Doctor of Philosophy.
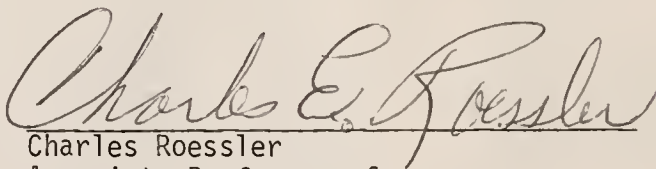
Lawrence T. Fitzgerald, Co-Chairman
Assistant Professor of
Nuclear Engineering Sciences

I certify that I have read this study and that in my opinion it conforms to acceptable standards of scholarly presentation and is fully adequate, in scope and quality, as a dissertation for the degree of Doctor of Philosophy.

Genevieve Roessler
Assistant Professor of
Nuclear Engineering Sciences

I certify that I have read this study and that in my opinion it conforms to acceptable standards of scholarly presentation and is fully adequate, in scope and quality, as a dissertation for the degree of Doctor of Philosophy.
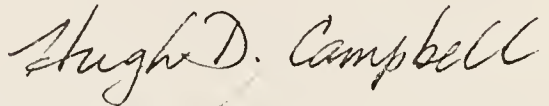
Charles Roessler
Associate Professor of
Environmental Engineering Sciences

I certify that I have read this study and that in my opinion it conforms to acceptable standards of scholarly presentation and is fully adequate, in scope and quality, as a dissertation for the degree of Doctor of Philosophy.

Rodney R. Million
Professor and Chief of
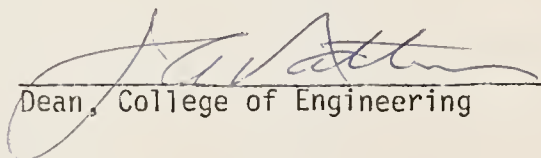   Division of Radiation Therapy

I certify that I have read this study and that in my opinion it conforms to acceptable standards of scholarly presentation and is fully adequate in scope and quality, as a dissertation for the degree of Doctor of Philosophy.

Hugh Campbell
Associate Professor of
    Nuclear Engineering Sciences

This dissertation was submitted to the Graduate Faculty of the College of Engineering and to the Graduate Council, and was accepted as partial fulfillment of the requirements for the degree of Doctor of Philosophy.

December 1977

Dean, College of Engineering

Dean, Graduate School